Analysis of functionally graded sandwich plates using a new first-order shear deformation theory

Huu-Tai Thai [a,*], Trung-Kien Nguyen[b], Thuc P. Vo [c], Jaehong Lee [d]

[a] School of Civil and Environmental Engineering, The University of New South Wales, Sydney, NSW 2052, Australia

[b] Faculty of Civil Engineering and Applied Mechanics, University of Technical Education Ho Chi Minh City, 1 Vo Van Ngan Street, Thu Duc District, Ho Chi Minh City, Vietnam.

[c] Faculty of Engineering and Environment, Northumbria University, Newcastle upon Tyne, NE1 8ST, UK.

[d] Department of Architectural Engineering, Sejong University, 98 Kunja Dong, Kwangjin Ku, Seoul 143-747, Korea

Abstract

In this paper, a new first-order shear deformation theory is presented for functionally graded sandwich plates composed of functionally graded face sheets and an isotropic homogeneous core. By making a further assumption to the existing first-order shear deformation theory, the number of unknowns and governing equations of the present theory is reduced, thereby making it simple to use. In addition, the use of shear correction factor is no longer necessary in the present theory since the transverse shear stresses are directly computed from the transverse shear forces by using equilibrium equations. Equations of motion are derived from Hamilton's principle. Analytical solutions for bending, buckling and free vibration analysis of rectangular plates under various boundary conditions are presented. Verification studies show that the present first-order shear deformation theory is not only more accurate than the conventional one, but also comparable with higher-order shear deformation theories which have a greater number of unknowns.

Keywords: Functionally graded sandwich plate; plate theory; bending; buckling; free

* Corresponding author. Tel.: + 61 2 9385 5029.
E-mail address: t.thai@unsw.edu.au (H.T. Thai).

vibration

1. Introduction

Functionally graded materials (FGMs) are a class of composites that have continuous variation of material properties from one surface to another, and thus eliminating the stress concentration found in laminated composites. A typical FGM is made from a mixture of ceramic and metal. These materials are often isotropic but nonhomogeneous. The reason for interest in FGMs is that it may be possible to create certain types of FGM structures capable of adapting to operating conditions.

Sandwich structures composed of a core bonded to two face sheets are commonly used in the aerospace vehicles due to their outstanding bending rigidity, low specific weight, excellent vibration characteristics and good fatigue properties. However, the sudden change in the material properties from one layer to another can result in stress concentrations which often lead to delamination. To overcome this problem, the concept of functionally graded (FG) sandwich structures is proposed. In such materials, two face sheets are made from isotropic FGMs while the core is made from an isotropic homogeneous material. Thanks to the smooth and continuous variation in the properties of FGMs, the stress concentration which is found in laminated sandwich structures is eliminated in FG sandwich structures.

With the wide application of FG sandwich structures, understanding their responses becomes an essential task. Since the shear deformation effect is more pronounced in thick plates or plates made of advanced composites like FGM, shear deformation theories such as first-order shear deformation theory (FSDT) and higher-order shear deformation theories (HSDT) should be used to predict the responses of FG sandwich plates. The FSDT gives acceptable results but depends on the shear correction factor which is hard to determine since it depends on many parameters. Conversely, the HSDT

do not require shear correction factor, but its equations of motion are more complicated than those of the FSDT. It is observed from the literature that most studies on FG sandwich plates are based on HSDTs. Zenkour [1-2] used a sinusoidal shear deformation theory (SSDT) to study the bending, buckling and free vibration of FG sandwich plates with FG face sheets and a homogeneous core. The behavior of FG sandwich plates under thermal environment was also studied by Zenkour and his colleagues [3-5] using FSDT, SSDT and third-order shear deformation theory (TSDT) of Reddy [6]. Based on an accurate HSDT, Natarajan and Manickam [7] studied the bending and free vibration behavior of two types of FG sandwich plates, i.e. homogeneous face sheets with a FG core and FG face sheets with a homogenous core. Neves [8-10] developed HSDT to predict the behavior of FG sandwich plates. Recently, Xiang et al. [11] analyzed the free vibration of FG sandwich plates using a nth-order shear deformation theory and a meshless method, while Sobhy [12] investigated the buckling and free vibration of FG sandwich plates using various HSDTs. Thai and Choi [13] derived analytical solutions of a zeroth-order shear deformation theory for bending, buckling and free vibration analyses of FG sandwich plates under various boundary conditions.

It is should be noted that HSDTs are highly computational cost due to involving in many unknowns (e.g., theories Neves et al. [9-10] with nine unknowns and Natarajan and Manickam [7] with thirteen unknowns). To reduce computational cost, HSDTs with four unknowns were recently developed for FG sandwich plates (see Refs. [14-21]). Although the existing FSDT is widely used to develop finite element models due to its simplicity, its accuracy is strongly dependent on the proper value of the shear correction factor. As a result, it is inconvenient to use. In this paper, a new FSDT which eliminates the use of the shear correction factor is developed for FG sandwich plates composed of FG face sheets and an isotropic homogeneous core. By making a further assumption, the

number of unknowns and governing equations of the present FSDT is reduced, thus makes it simple to use. Equations of motion and boundary conditions are derived from Hamilton's principle. Analytical solutions for rectangular plates under various boundary conditions are obtained. Numerical examples are presented to verify the accuracy of the present theory in predicting the bending, buckling and free vibration responses of FG sandwich plates.

2. Theoretical formulation

Consider a sandwich plate composed of three layers as shown in Fig. 1. Two FG face sheets are made from a mixture of a metal and a ceramic, while a core is made of an isotropic homogeneous material. The material properties of FG face sheets are assumed to vary continuously through the plate thickness by a power law distribution as

$$P(z) = P_m + (P_c - P_m)V \tag{1}$$

where P represents the effective material property such as Young's modulus E, Poisson's ratio ν, and mass density ρ; subscripts c and m denote the ceramic and metal phases, respectively; and V is the volume fraction of the ceramic phase defined by

$$\begin{cases} V^{(1)}(z) = \left(\dfrac{z-h_0}{h_1-h_0}\right)^p & \text{for } z \in [h_0, h_1] \\ V^{(2)}(z) = 1 & \text{for } z \in [h_1, h_2] \\ V^{(3)}(z) = \left(\dfrac{z-h_3}{h_2-h_3}\right)^p & \text{for } z \in [h_2, h_3] \end{cases} \tag{2}$$

where p is the power law index that governs the volume fraction gradation. Fig. 2 shows the through thickness variation of the volume fraction of the ceramic phase for five different schemes considered in this study.

2.1. Kinematics

The displacement field of the conventional FSDT is given by

$$\begin{aligned} u_1(x,y,z) &= u(x,y) + z\varphi_x(x,y) \\ u_2(x,y,z) &= v(x,y) + z\varphi_y(x,y) \\ u_3(x,y,z) &= w(x,y) \end{aligned} \tag{3}$$

where u, v, w, φ_x and φ_y are five unknown displacement functions of the midplane of the plate. By assuming $\varphi_x = -\partial\theta/\partial x$ and $\varphi_y = -\partial\theta/\partial y$, the displacement field of the new FSDT can be rewritten in a simpler form as

$$\begin{aligned} u_1(x,y,z) &= u(x,y) - z\frac{\partial\theta}{\partial x} \\ u_2(x,y,z) &= v(x,y) - z\frac{\partial\theta}{\partial y} \\ u_3(x,y,z) &= w(x,y) \end{aligned} \tag{4}$$

It is clear that the displacement field in Eq. (4) contains only four unknowns (u, v, θ, w). It is worth noting that the simple FSDT recently proposed by Thai and Choi [22-23] also involves only four unknowns like the present theory. However, the displacement field of the simple FSDT [22-23] is obtained by splitting the transverse displacement into bending and shear parts instead of using a further assumption as in the present work. Therefore, the displacement field and subsequent equations of motion derived in this study will be completely different with those given by Thai and Choi [22-23]. In addition, the present FSDT does not require a shear correction factor as in the case of the simple FSDT [22-23].

The strains associated with the displacement field in Eq. (4) are:

$$\begin{Bmatrix} \varepsilon_x \\ \varepsilon_y \\ \gamma_{xy} \end{Bmatrix} = \begin{Bmatrix} \varepsilon_x^0 \\ \varepsilon_y^0 \\ \gamma_{xy}^0 \end{Bmatrix} + z\begin{Bmatrix} \kappa_x \\ \kappa_y \\ \kappa_{xy} \end{Bmatrix} \tag{5a}$$

$$\begin{Bmatrix} \gamma_{xz} \\ \gamma_{yz} \end{Bmatrix} = \begin{Bmatrix} \gamma_{xz}^0 \\ \gamma_{yz}^0 \end{Bmatrix} \tag{5b}$$

Eq. (5) can be rewritten in a compact form as

$$\{\varepsilon\} = \{\varepsilon^0\} + z\{\kappa\} \tag{6a}$$

$$\{\gamma\} = \{\gamma^0\} \tag{6b}$$

where

$$\{\varepsilon^0\} = \begin{Bmatrix} \varepsilon_x^0 \\ \varepsilon_y^0 \\ \gamma_{xy}^0 \end{Bmatrix} = \begin{Bmatrix} \dfrac{\partial u}{\partial x} \\ \dfrac{\partial v}{\partial y} \\ \dfrac{\partial u}{\partial y} + \dfrac{\partial v}{\partial x} \end{Bmatrix}, \{\kappa\} = \begin{Bmatrix} \kappa_x \\ \kappa_y \\ \kappa_{xy} \end{Bmatrix} = \begin{Bmatrix} -\dfrac{\partial^2 \theta}{\partial x^2} \\ -\dfrac{\partial^2 \theta}{\partial y^2} \\ -2\dfrac{\partial^2 \theta}{\partial x \partial y} \end{Bmatrix}, \{\gamma^0\} = \begin{Bmatrix} \gamma_{xz}^0 \\ \gamma_{yz}^0 \end{Bmatrix} = \begin{Bmatrix} \dfrac{\partial w}{\partial x} - \dfrac{\partial \theta}{\partial x} \\ \dfrac{\partial w}{\partial y} - \dfrac{\partial \theta}{\partial y} \end{Bmatrix} \tag{7}$$

2.2. Constitutive equations

The linear elastic constitutive equations of FG sandwich plates can be written as

$$\begin{Bmatrix} \sigma_x \\ \sigma_y \\ \sigma_{xy} \end{Bmatrix} = \begin{bmatrix} C_{11} & C_{12} & 0 \\ C_{12} & C_{22} & 0 \\ 0 & 0 & C_{66} \end{bmatrix} \begin{Bmatrix} \varepsilon_x \\ \varepsilon_y \\ \varepsilon_{xy} \end{Bmatrix} \tag{8a}$$

$$\begin{Bmatrix} \sigma_{xz} \\ \sigma_{yz} \end{Bmatrix} = \begin{bmatrix} C_{55} & 0 \\ 0 & C_{44} \end{bmatrix} \begin{Bmatrix} \gamma_{xz} \\ \gamma_{yz} \end{Bmatrix} \tag{8b}$$

where

$$\begin{aligned} C_{11}(z) = C_{22}(z) &= \frac{E(z)}{1-\nu(z)^2},\ C_{12}(z) = \nu(z) C_{11}(z) \\ C_{44}(z) = C_{55}(z) = C_{66}(z) &= \frac{E(z)}{2\left[1+\nu(z)\right]} \end{aligned} \tag{9}$$

2.3. Equations of motion

Hamilton's principle is used herein to derive equations of motion. The principle can be stated in an analytical form as

$$0 = \int_0^T \left(\delta U + \delta V - \delta K \right) dt \tag{10}$$

where δU, δV, and δK are the variations of strain energy, work done, and kinetic energy, respectively. The variation of strain energy is calculated by

$$\begin{aligned} \delta U &= \int_A \int_{-h/2}^{h/2} \left(\sigma_x \delta \varepsilon_x + \sigma_y \delta \varepsilon_y + \sigma_{xy} \delta \gamma_{xy} + \sigma_{xz} \delta \gamma_{xz} + \sigma_{yz} \delta \gamma_{yz} \right) dA dz \\ &= \int_A \left[N_x \frac{\partial \delta u}{\partial x} - M_x \frac{\partial^2 \delta \theta}{\partial x^2} + N_y \frac{\partial \delta v}{\partial y} - M_y \frac{\partial^2 \delta \theta}{\partial y^2} \right. \\ &\quad \left. + N_{xy} \left(\frac{\partial \delta u}{\partial y} + \frac{\partial \delta v}{\partial x} \right) - 2 M_{xy} \frac{\partial^2 \delta \theta}{\partial x \partial y} + Q_x \frac{\partial \delta \left(w - \theta \right)}{\partial x} + Q_y \frac{\partial \delta \left(w - \theta \right)}{\partial y} \right] dA \end{aligned} \tag{11}$$

where N, M, and Q are the stress resultants defined by

$$\left(N_x, N_y, N_{xy} \right) = \int_{-h/2}^{h/2} \left(\sigma_x, \sigma_y, \sigma_{xy} \right) dz \tag{12a}$$

$$\left(M_x, M_y, M_{xy} \right) = \int_{-h/2}^{h/2} \left(\sigma_x, \sigma_y, \sigma_{xy} \right) z dz \tag{12b}$$

$$\left(Q_x, Q_y \right) = \int_{-h/2}^{h/2} \left(\sigma_{xz}, \sigma_{yz} \right) dz \tag{12c}$$

The variation of work done by transverse load q and in-plane load $\left(N_x^0, N_y^0, N_{xy}^0 \right)$ can be expressed as

$$\delta V = -\int_A q \delta w dA + \int_A \left(N_x^0 \frac{\partial w}{\partial x} \frac{\partial \delta w}{\partial x} + N_y^0 \frac{\partial w}{\partial y} \frac{\partial \delta w}{\partial y} + 2 N_{xy}^0 \frac{\partial w}{\partial x} \frac{\partial \delta w}{\partial y} \right) dA \tag{13}$$

The variation of kinetic energy can be written as

$$\begin{aligned} \delta K &= \int_V \left(\ddot{u}_1 \delta u_1 + \ddot{u}_2 \delta u_2 + \ddot{u}_3 \delta u_3 \right) \rho \left(z \right) dA dz \\ &= \int_A \left\{ I_0 \left[\ddot{u} \delta u + \ddot{v} \delta v + \ddot{w} \delta w \right] \right. \\ &\quad \left. - I_1 \left(\ddot{u} \frac{\partial \delta \theta}{\partial x} + \frac{\partial \ddot{\theta}}{\partial x} \delta u + \ddot{v} \frac{\partial \delta \theta}{\partial y} + \frac{\partial \ddot{\theta}}{\partial y} \delta v \right) + I_2 \left(\frac{\partial \ddot{\theta}}{\partial x} \frac{\partial \delta \theta}{\partial x} + \frac{\partial \ddot{\theta}}{\partial y} \frac{\partial \delta \theta}{\partial y} \right) \right\} dA \end{aligned} \tag{14}$$

where dot-superscript convention indicates the differentiation with respect to the time

variable t, $\rho(z)$ is the mass density, and (I_0, I_1, I_2) are mass inertias defined by

$$(I_0, I_1, I_2) = \int_{-h/2}^{h/2} (1, z, z^2)\rho(z)dz = \sum_{n=1}^{3} \int_{h_{n-1}}^{h_n} (1, z, z^2)\rho^{(n)}(z)dz \tag{15}$$

Substituting the expressions for δU, δV, and δK from Eqs. (11), (13), and (14) into Eq. (10) and integrating by parts, and collecting the coefficients of δu, δv, $\delta\theta$, and δw, the following equations of motion are obtained:

$$\delta u: \ \frac{\partial N_x}{\partial x} + \frac{\partial N_{xy}}{\partial y} = I_0 \ddot{u} - I_1 \frac{\partial \ddot{\theta}}{\partial x} \tag{16a}$$

$$\delta v: \ \frac{\partial N_{xy}}{\partial x} + \frac{\partial N_y}{\partial y} = I_0 \ddot{v} - I_1 \frac{\partial \ddot{\theta}}{\partial y} \tag{16b}$$

$$\delta\theta: \frac{\partial^2 M_x}{\partial x^2} + 2\frac{\partial^2 M_{xy}}{\partial x \partial y} + \frac{\partial^2 M_y}{\partial y^2} - \left(\frac{\partial Q_x}{\partial x} + \frac{\partial Q_y}{\partial y} \right) = I_1 \left(\frac{\partial \ddot{u}}{\partial x} + \frac{\partial \ddot{v}}{\partial y} \right) - I_2 \nabla^2 \ddot{\theta} \tag{16c}$$

$$\delta w: \frac{\partial Q_x}{\partial x} + \frac{\partial Q_y}{\partial y} + q + N_x^0 \frac{\partial^2 w}{\partial x^2} + N_y^0 \frac{\partial^2 w}{\partial y^2} + 2N_{xy}^0 \frac{\partial^2 w}{\partial x \partial y} = I_0 \ddot{w} \tag{16d}$$

The natural boundary conditions are of the form:

$$\delta u: N_x n_x + N_{xy} n_y \tag{17a}$$

$$\delta v: N_{xy} n_x + N_y n_y \tag{17b}$$

$$\delta\theta: \frac{\partial M_n}{\partial n} + 2\frac{\partial M_{ns}}{\partial s} + Q_x n_x + Q_y n_y - I_1 (\ddot{u} n_x + \ddot{v} n_y) + I_2 \frac{\partial \ddot{\theta}}{\partial n} \tag{17c}$$

$$\delta w: \left(Q_x + N_x^0 \frac{\partial w}{\partial x} + N_{xy}^0 \frac{\partial w}{\partial y} \right) n_x + \left(Q_y + N_{xy}^0 \frac{\partial w}{\partial x} + N_y^0 \frac{\partial w}{\partial y} \right) n_y \tag{17d}$$

$$\frac{\partial \delta\theta}{\partial n}: M_n \tag{17e}$$

where

$$M_n = M_x n_x^2 + M_y n_y^2 + 2M_{xy} n_x n_y \tag{18a}$$

$$M_{ns} = \left(M_y - M_x\right) n_x n_y + M_{xy}\left(n_x^2 - n_y^2\right) \tag{18b}$$

$$\frac{\partial}{\partial n} = n_x \frac{\partial}{\partial x} + n_y \frac{\partial}{\partial y}, \quad \frac{\partial}{\partial s} = n_x \frac{\partial}{\partial y} - n_y \frac{\partial}{\partial x} \tag{18c}$$

with n_x and n_y being the direction cosines of the unit normal to the boundary of the middle plane. The above boundary conditions can be rewritten in an explicit form as

clamped edge

$$u = v = \theta = w = \frac{\partial \theta}{\partial x} = 0, \text{ at } \; x = 0, a \tag{19a}$$

$$u = v = \theta = w = \frac{\partial \theta}{\partial y} = 0, \text{ at } \; y = 0, b \tag{19b}$$

simply supported edge

$$N_x = v = \theta = w = M_x = 0, \text{ at } \; x = 0, a \tag{20a}$$

$$u = N_y = \theta = w = M_y = 0, \text{ at } \; y = 0, b \tag{20b}$$

and free edge

$$N_x = N_{xy} = \frac{\partial M_x}{\partial x} + 2\frac{\partial M_{xy}}{\partial y} - I_1 \ddot{u} + I_2 \frac{\partial \ddot{\theta}}{\partial x} = Q_x + N_x^0 \frac{\partial w}{\partial x} + N_{xy}^0 \frac{\partial w}{\partial y} = M_x = 0, \text{ at } \; x = 0, a \tag{21a}$$

$$N_{xy} = N_y = 2\frac{\partial M_{xy}}{\partial x} + \frac{\partial M_y}{\partial y} - I_1 \ddot{u} + I_2 \frac{\partial \ddot{\theta}}{\partial y} = Q_y + N_{xy}^0 \frac{\partial w}{\partial x} + N_y^0 \frac{\partial w}{\partial y} = M_y = 0, \text{ at } \; y = 0, b \tag{21b}$$

Substituting Eq. (5a) into Eq. (8a) and the subsequent results into Eqs. (12a)-(12b), the axial forces N and bending moments M are obtained in terms of strains as

$$\begin{Bmatrix} N_x \\ N_y \\ N_{xy} \end{Bmatrix} = \begin{bmatrix} A_{11} & A_{12} & 0 \\ A_{12} & A_{22} & 0 \\ 0 & 0 & A_{66} \end{bmatrix} \begin{Bmatrix} \varepsilon_x^0 \\ \varepsilon_y^0 \\ \gamma_{xy}^0 \end{Bmatrix} + \begin{bmatrix} B_{11} & B_{12} & 0 \\ B_{12} & B_{22} & 0 \\ 0 & 0 & B_{66} \end{bmatrix} \begin{Bmatrix} \kappa_x \\ \kappa_y \\ \kappa_{xy} \end{Bmatrix} \tag{22a}$$

$$\begin{Bmatrix} M_x \\ M_y \\ M_{xy} \end{Bmatrix} = \begin{bmatrix} B_{11} & B_{12} & 0 \\ B_{12} & B_{22} & 0 \\ 0 & 0 & B_{66} \end{bmatrix} \begin{Bmatrix} \varepsilon_x^0 \\ \varepsilon_y^0 \\ \gamma_{xy}^0 \end{Bmatrix} + \begin{bmatrix} D_{11} & D_{12} & 0 \\ D_{12} & D_{22} & 0 \\ 0 & 0 & D_{66} \end{bmatrix} \begin{Bmatrix} \kappa_x \\ \kappa_y \\ \kappa_{xy} \end{Bmatrix} \tag{22b}$$

where $\left(A_{ij}, B_{ij}, D_{ij}\right)$ are the stiffness coefficients defined by

$$\left(A_{ij}, B_{ij}, D_{ij}\right) = \int_{-h/2}^{h/2} \left(1, z, z^2\right) C_{ij}\left(z\right) dz = \sum_{n=1}^{3} \int_{h_{n-1}}^{h_n} \left(1, z, z^2\right) C_{ij}^{(n)}\left(z\right) dz \tag{23}$$

Eq. (22) can be rewritten in a compact form as

$$\begin{Bmatrix} \{N\} \\ \{M\} \end{Bmatrix} = \begin{bmatrix} [A] & [B] \\ [B] & [D] \end{bmatrix} \begin{Bmatrix} \{\varepsilon^0\} \\ \{\kappa\} \end{Bmatrix} \tag{24}$$

It should be noted that the transverse shear stresses $\left(\sigma_{xz}, \sigma_{yz}\right)$ computed from the constitutive equation Eq. (8b) violate the zero transverse shear stress conditions on the top and bottom surfaces of the plate. A shear correction factor is therefore required. To avoid the use of the shear correction factor, equilibrium equations are used herein. The equilibrium equations of a body is given by

$$\frac{\partial \sigma_x}{\partial x} + \frac{\partial \sigma_{xy}}{\partial y} + \frac{\partial \sigma_{xz}}{\partial z} = 0 \tag{25a}$$

$$\frac{\partial \sigma_{xy}}{\partial x} + \frac{\partial \sigma_y}{\partial y} + \frac{\partial \sigma_{yz}}{\partial z} = 0 \tag{25b}$$

$$\frac{\partial \sigma_{xz}}{\partial x} + \frac{\partial \sigma_{yz}}{\partial y} + \frac{\partial \sigma_z}{\partial z} = 0 \tag{25c}$$

The transverse shear stresses can be derived from Eqs. (25a) and (25b) as

$$\sigma_{xz} = -\int_{-h/2}^{z} \left(\frac{\partial \sigma_x}{\partial x} + \frac{\partial \sigma_{xy}}{\partial y} \right) d\varsigma \tag{26a}$$

$$\sigma_{yz} = -\int_{-h/2}^{z} \left(\frac{\partial \sigma_{xy}}{\partial x} + \frac{\partial \sigma_y}{\partial y} \right) d\varsigma \tag{26b}$$

The in-plane stresses $\left(\sigma_x, \sigma_y, \sigma_{xy}\right)$ are computed from constitutive equations Eq. (8a) as

$$\{\sigma\}=[C]\{\varepsilon\}=[C]\left(\left\{\varepsilon^0\right\}+z\{\kappa\}\right) \tag{27}$$

where the axial strain $\left\{\varepsilon^0\right\}$ and the curvature $\{\kappa\}$ are related to the axial force $\{N\}$ and bending moment $\{M\}$ by the inversion of Eq. (24)

$$\begin{Bmatrix}\left\{\varepsilon^0\right\}\\ \{\kappa\}\end{Bmatrix}=\begin{bmatrix}[a] & [b]\\ [b] & [d]\end{bmatrix}\begin{Bmatrix}\{N\}\\ \{M\}\end{Bmatrix} \tag{28}$$

Substituting Eq. (28) into Eq. (27), the in-plane stresses can be rewritten as

$$\{\sigma\}=[C]\left\{\left([a]+z[b]\right)\{N\}+\left([b]+z[d]\right)\{M\}\right\} \tag{29}$$

Substituting Eq. (29) into Eq. (26), using equilibrium equations of the plate, assuming two cylindrical bending modes, and omitting the weak terms, the following transverse shear stresses are obtained [24]

$$\sigma_{xz}=\bar{m}_{11}(z)Q_x \tag{30a}$$

$$\sigma_{yz}=\bar{m}_{22}(z)Q_y \tag{30b}$$

where

$$\bar{m}_{11}=-\int_{-h/2}^{z}\left[C_{11}\left(b_{11}+\varsigma d_{11}\right)+C_{12}\left(b_{21}+\varsigma d_{21}\right)\right]d\varsigma \tag{31a}$$

$$\bar{m}_{22}=-\int_{-h/2}^{z}\left[C_{12}\left(b_{12}+\varsigma d_{12}\right)+C_{22}\left(b_{22}+\varsigma d_{22}\right)\right]d\varsigma \tag{31b}$$

By using the shear stresses defined in Eq. (30a), the shear deformation energy per unit middle surface area is then given by the following expression:

$$\Pi_s=\frac{1}{2}\int_{-h/2}^{h/2}\sigma_{xz}\gamma_{xz}dz=\frac{1}{2}Q_x^2\int_{-h/2}^{h/2}\frac{\bar{m}_{11}^2(z)}{C_{55}(z)}dz \tag{32}$$

The shear deformation energy per unit middle surface area can be also calculated using the average shear deformation,

$$\Pi_{sa} = \frac{1}{2} Q_x \gamma_{xz}^0 = \frac{1}{2} \frac{Q_x^2}{H_{55}} \tag{33}$$

By considering of the balance of the transverse shear strain energy in Eqs. (32) and (33), the transverse shear stiffness H_{55} is obtained as

$$H_{55} = \left(\int_{-h/2}^{h/2} \frac{\bar{m}_{11}^2(z)}{C_{55}(z)} dz \right)^{-1} = \left(\sum_{n=1}^{3} \int_{h_{n-1}}^{h_n} \frac{\left[\bar{m}_{11}^{(n)}(z) \right]^2}{C_{55}^{(n)}(z)} dz \right)^{-1} \tag{34}$$

Similarly, the transverse shear stiffness H_{44} can be obtained as

$$H_{44} = \left(\int_{-h/2}^{h/2} \frac{\bar{m}_{22}^2(z)}{C_{44}(z)} dz \right)^{-1} = \left(\sum_{n=1}^{3} \int_{h_{n-1}}^{h_n} \frac{\left[\bar{m}_{22}^{(n)}(z) \right]^2}{C_{44}^{(n)}(z)} dz \right)^{-1} \tag{35}$$

Then, the transverse shear forces based on equilibrium equations are given as follow

$$\begin{Bmatrix} Q_x \\ Q_y \end{Bmatrix} = \begin{bmatrix} H_{55} & 0 \\ 0 & H_{44} \end{bmatrix} \begin{Bmatrix} \gamma_{xz}^0 \\ \gamma_{yz}^0 \end{Bmatrix} \tag{36}$$

It should be noted that $H_{44} = H_{55} = H$ due to the isotropic properties of FGMs. The equations of motion of the present FSDT can be expressed in terms of displacements (u, v, θ, w) by substituting Eq. (7) into Eqs. (22) and (36) and the subsequent results into Eq. (16)

$$A_{11}\frac{\partial^2 u}{\partial x^2} + A_{66}\frac{\partial^2 u}{\partial y^2} + (A_{12} + A_{66})\frac{\partial^2 v}{\partial x \partial y} - B_{11}\frac{\partial^3 \theta}{\partial x^3} - (B_{12} + 2B_{66})\frac{\partial^3 \theta}{\partial x \partial y^2} = I_0 \ddot{u} - I_1 \frac{\partial \ddot{\theta}}{\partial x} \tag{37a}$$

$$A_{22}\frac{\partial^2 v}{\partial y^2} + A_{66}\frac{\partial^2 v}{\partial x^2} + (A_{12} + A_{66})\frac{\partial^2 u}{\partial x \partial y} - B_{22}\frac{\partial^3 \theta}{\partial y^3} - (B_{12} + 2B_{66})\frac{\partial^3 \theta}{\partial x^2 \partial y} = I_0 \ddot{v} - I_1 \frac{\partial \ddot{\theta}}{\partial y} \tag{37b}$$

$$\begin{aligned} &B_{11}\frac{\partial^3 u}{\partial x^3} + (B_{12} + 2B_{66})\frac{\partial^3 u}{\partial x \partial y^2} + (B_{12} + 2B_{66})\frac{\partial^3 v}{\partial x^2 \partial y} + B_{22}\frac{\partial^3 v}{\partial y^3} - D_{11}\frac{\partial^4 \theta}{\partial x^4} \\ &-2(D_{12} + 2D_{66})\frac{\partial^4 \theta}{\partial x^2 \partial y^2} - D_{22}\frac{\partial^4 \theta}{\partial y^4} - H\nabla^2(w - \theta) = I_1\left(\frac{\partial \ddot{u}}{\partial x} + \frac{\partial \ddot{v}}{\partial y}\right) - I_2 \nabla^2 \ddot{\theta} \end{aligned} \tag{37c}$$

$$H\nabla^2(w-\theta)+q+N_x^0\frac{\partial^2 w}{\partial x^2}+N_y^0\frac{\partial^2 w}{\partial y^2}+2N_{xy}^0\frac{\partial^2 w}{\partial x\partial y}=I_0\ddot{w} \tag{37d}$$

3. Analytical solutions

Consider a rectangular plate with length a and width b under transverse load q and in-plane forces in two directions ($N_x^0=\gamma_1 N_{cr}, N_y^0=\gamma_2 N_{cr}, N_{xy}^0=0$). The analytical solution of Eq. (37) can be obtained for rectangular plates under various boundary conditions by using the following expansions of generalized displacements

$$\begin{aligned} u(x,y,t)&=U_{mn}X'(x)Y(y)e^{i\omega t}\\ v(x,y,t)&=V_{mn}X(x)Y'(y)e^{i\omega t}\\ \theta(x,y,t)&=\phi_{mn}X(x)Y(y)e^{i\omega t}\\ w(x,y,t)&=W_{mn}X(x)Y(y)e^{i\omega t} \end{aligned} \tag{38}$$

where $i=\sqrt{-1}$, $(U_{mn},V_{mn},\phi_{mn},W_{mn})$ are coefficients, and ω is the natural frequency. The functions $X(x)$ and $Y(y)$ given in Table 1 are suggested by Sobhy [12] to satisfy various boundary conditions in Eqs. (19) – (21).

The transversely load q is also chosen as

$$q(x,y)=Q_{mn}\sin\alpha x\sin\beta y \tag{39}$$

where the coefficients Q_{mn} are given below for certain typical loads:

$$Q_{mn}=\begin{cases} q_0 & \text{for sinusoidal loads}\\ \dfrac{16q_0}{mn\pi^2} & \text{for uniform loads}\end{cases} \tag{40}$$

with $\alpha=m\pi/a$, $\beta=n\pi/b$.

Substituting Eqs. (38) and (40) into Eq. (37), the analytical solutions can be obtained from

$$\left(\begin{bmatrix} k_{11} & k_{12} & k_{13} & 0 \\ k_{21} & k_{22} & k_{23} & 0 \\ k_{31} & k_{32} & k_{33} & k_{34} \\ 0 & 0 & k_{34} & k_{44}+\lambda \end{bmatrix} - \omega^2 \begin{bmatrix} m_{11} & 0 & m_{13} & 0 \\ 0 & m_{22} & m_{23} & 0 \\ m_{13} & m_{23} & m_{33} & 0 \\ 0 & 0 & 0 & m_{44} \end{bmatrix} \right) \begin{Bmatrix} U_{mn} \\ V_{mn} \\ W_{bmn} \\ W_{smn} \end{Bmatrix} = \begin{Bmatrix} 0 \\ 0 \\ 0 \\ f_q \end{Bmatrix} \tag{41}$$

where

$$k_{11} = -\int_0^a \int_0^b \left(A_{11} X''' Y + A_{66} X' Y'' \right) X' Y dxdy, \quad k_{12} = -\int_0^a \int_0^b \left(A_{12} + A_{66} \right) X' Y'' X' Y dxdy$$
$$k_{13} = \int_0^a \int_0^b \left[B_{11} X''' Y + \left(B_{12} + 2B_{66} \right) X' Y'' \right] X' Y dxdy \tag{42a}$$

$$k_{21} = -\int_0^a \int_0^b \left(A_{12} + A_{66} \right) X'' Y' X Y' dxdy, \quad k_{22} = -\int_0^a \int_0^b \left(A_{22} X Y''' + A_{66} X'' Y' \right) X Y' dxdy$$
$$k_{23} = \int_0^a \int_0^b \left[B_{22} X Y''' + \left(B_{12} + 2B_{66} \right) X'' Y' \right] X Y' dxdy \tag{42b}$$

$$k_{31} = -\int_0^a \int_0^b \left[B_{11} X''' Y + \left(B_{12} + 2B_{66} \right) X'' Y'' \right] X Y dxdy$$
$$k_{32} = -\int_0^a \int_0^b \left[B_{22} X Y''' + \left(B_{12} + 2B_{66} \right) X'' Y'' \right] X Y dxdy$$
$$k_{33} = \int_0^a \int_0^b \left[D_{11} X''' Y + 2\left(D_{12} + 2D_{66} \right) X'' Y'' + D_{22} X Y''' - H\left(X'' Y + X Y'' \right) \right] X Y dxdy \tag{42c}$$
$$k_{34} = \int_0^a \int_0^b H\left(X'' Y + X Y'' \right) X Y dxdy, \quad k_{44} = -k_{34}$$

$$\lambda = -N_{cr} \int_0^a \int_0^b \left(\gamma_1 X'' Y + \gamma_2 X Y'' \right) X Y dxdy \tag{42d}$$

$$f_q = Q_{mn} \int_0^a \int_0^b \sin \alpha x \sin \beta y \sin \alpha x \sin \beta y dxdy \tag{42e}$$

$$m_{11} = I_0 \int_0^a \int_0^b X' Y X' Y dxdy, \qquad m_{22} = I \int_0^a \int_0^b X Y' X Y' dxdy$$
$$m_{13} = -I_1 \int_0^a \int_0^b X' Y X' Y dxdy, \qquad m_{23} = -I_1 \int_0^a \int_0^b X Y' X Y' dxdy \tag{42f}$$

$$m_{31} = I_1 \int_0^a \int_0^b X'' Y X Y dxdy, \qquad m_{32} = I_1 \int_0^a \int_0^b X Y'' X Y dxdy$$
$$m_{33} = -I_2 \int_0^a \int_0^b \left(X'' Y + X Y'' \right) X Y dxdy, \quad m_{44} = I_0 \int_0^a \int_0^b X Y X Y dxdy \tag{42g}$$

4. Numerical examples

In this section, a number of numerical examples are presented and discussed to verify the accuracy of the present theory and investigate the effects of the power law index,

thickness ratio of layers, i.e. scheme, and transverse shear deformation on deflection, critical buckling load and natural frequency of FG sandwich plates. Unless mentioned otherwise, a simply supported Al/Al_2O_3 sandwich plate composed of aluminum face sheets (as metal) and an alumina core (as ceramic) under sinusoidal loads is considered. Young's modulus, Poisson's ratio and density of aluminum are $E_m = 70\,\text{GPa}$, $\nu_m = 0.3$ and $\rho_m = 2702\,\text{kg/m}^3$, respectively, and those of alumina are $E_c = 380\,\text{GPa}$, $\nu_c = 0.3$ and $\rho_c = 3800\,\text{kg/m}^3$. Five different schemes of sandwich plate are considered (see Fig. 2). For convenience, the ratio of the thickness of each layer from bottom to top is denoted by the combination of three numbers, i.e. (1-0-1), (2-1-2) and so on. A four-letter notation as shown in Table 1 is used to describe the boundary conditions of the plate. The following dimensionless forms are used:

$$\begin{aligned}
&\hat{w} = \frac{10E_0 h}{q_0 a^2} w\left(\frac{a}{2},\frac{b}{2}\right),\ \bar{\sigma}_x(z) = \frac{10h^2}{q_0 a^2}\sigma_x\left(\frac{a}{2},\frac{b}{2},z\right),\ \bar{\sigma}_{xz}(z) = \frac{h}{q_0 a}\sigma_{xz}\left(0,\frac{b}{2},z\right)\\
&\bar{w} = \frac{10E_c h^3}{q_0 a^4} w\left(\frac{a}{2},\frac{b}{2}\right),\ \bar{N} = \frac{N_{cr}a^2}{100E_0 h^3},\ \bar{\omega} = \omega\frac{a^2}{h}\sqrt{\rho_0/E_0},\ E_0 = 1\text{GPa},\ \rho_0 = 1\text{kg/m}^3
\end{aligned} \tag{43}$$

4.1. Verification studies

Example 1. The first example aims to verify the accuracy of the present theory in predicting the bending responses of FG sandwich plates. A moderately thick square plate with the thickness ratio equal to 10 and the power law index varied from 0 to 10 is analyzed. The ceramic core of FG sandwich plate is made of zirconia (ZrO_2) with Young's modulus and Poisson's ratio being 151 GPa and 0.3, respectively. The obtained results are compared with those generated by Zenkour [1] based on the SSDT, TSDT and FSDT in Tables 2-4 and Figs. 3 and 4. It is clear that the conventional FSDT [1] violates the stress-free boundary conditions on the plate surface (Fig. 4), and consequently, a shear correction factor is required. In general, a good agreement

between the results is found (see Tables 2 and 3 and Fig. 3), except for the case of transverse shear stress $\bar{\sigma}_{xz}$ where a small difference between the results is seen (see Table 4 and Fig. 4). This is due to the different approaches used to predict the transverse shear stresses. In this study, the transverse shear stresses are obtained using equilibrium equations while those given by Zenkour [1] are computed from constitutive equations. Finally, it is important to note that the present theory involves only four unknowns as against five in the case of SSDT, TSDT and FSDT. Besides, it does not require a shear correction factor as in the case of FSDT. Therefore, it can be stated that the present theory is not only accurate but also simple in predicting the bending behavior of FG sandwich plates.

Example 2. The aim of this example is to verify the accuracy of the present theory in predicting the critical buckling load of FG sandwich plates. A moderately thick square plate with the thickness ratio equal to 10 and the power law index varied from 0 to 10 is analyzed. Dimensionless critical buckling loads $\bar{N}$ of square plates under uniaxial and biaxial compressions are presented in Table 5 and Table 6, respectively. The obtained results are compared with those generated by El Meiche et al. [16] based on the HSDT and Zenkour [2] based on the SSDT, TSDT and FSDT. An excellent agreement between the results is obtained for all schemes and values of power law index. It should be recalled that the present theory contains only four unknowns and four governing equations, while the number of unknowns and governing equations of the HSDT, SSDT, TSDT and FSDT is five. Thus, it can be stated that the present model is not only accurate but also simple in predicting the critical buckling load of FG sandwich plates.

Further verification of critical buckling loads is displayed in Fig. 5 for thick plates. In this figure, the variations of dimensionless critical buckling loads versus thickness ratio

a/h are compared for (1-2-1) FG sandwich rectangular plates under both uniaxial and biaxial compressions. It can be seen that the present solutions agree well with the TSDT solutions [2] even for the case of very thick plates where the shear deformation effect is more pronounced. Whereas, the FSDT [2] gives acceptable results for moderately thick plates only. For thick or very thick plates with the thickness ratio $a/h<5$, a slightly difference between the results predicted by the FSDT and TSDT is observed. It is due to the fact that the FSDT is unable to predict accurately the responses of plates with the mentioned thickness ratio ($a/h<5$).

Example 3. The last example aims to verify the accuracy of the present theory in predicting the natural frequency of FG sandwich plates. Table 7 contains dimensionless fundamental frequency $\bar{\omega}$ of a moderately thick square plate with the thickness ratio equal to 10. The obtained results are compared with three-dimensional (3D) solutions [25] and those predicted by HSDT [16], SSDT [2], TSDT [2] and FSDT [2]. It can be seen that the present solutions are in excellent agreement with the existing results and even more accurate than those predicted by the conventional FSDT [2]. For example, with $p=10$, when compared with exact 3D solutions [25], the maximum error of the present FSDT is only 0.29 % for the (1-0-1) FG sandwich plate, whereas the maximum error of the conventional FSDT [2] is 3.92 % for the (2-2-1) one.

To verify for higher order modes, Table 8 shows the comparison of the first ten natural frequencies of (1-2-1) and (2-2-1) FG sandwich plates. The thickness ratio a/h and power law index p of the plate are taken as 10 and 2, respectively. The obtained results are compared with those predicted by HSDT [16], SSDT [2], TSDT [2] and FSDT [2]. As expected, a good agreement between the results is obtained for all vibration modes which confirm the accuracy of the present theory.

To verify for thick plates, Table 9 shows dimensionless fundamental frequency $\bar{\omega}$ of a thick square plate with the thickness ratio equal to 5. Two cases of FG sandwich plates are considered: (1) ceramic core (hardcore) and (2) metal core (softcore). Dimensionless fundamental frequencies predicted by the present theory using equilibrium equations without using shear correction factor and constitutive equations with a shear correction factor $k = 5/6$ are compared with exact 3D solutions reported by Li et al. [25]. In general, the present theory using equilibrium equations gives a good prediction of frequency of FG sandwich plates with both hardcore and softcore. Whereas, the present theory with $k = 5/6$ gives a good prediction of frequency of FG sandwich plates with hardcore only, but there are some errors in the case of FG sandwich plates with softcore. For example, with $p = 10$, when compared with exact 3D solutions [25], the errors of the present theory with $k = 5/6$ are 1.24 % and 11.94 % for (1-2-1) FG sandwich plates with hardcore and softcore, respectively. This indicates that the use of a constant shear correction factor is not appropriate for the case of FG sandwich plates with softcore. This statement can be clearly seen in Fig. 6 in which the frequency ratio is defined as the ratio of the frequency from the present model and that from the FSDT with $k = 5/6$. For FG sandwich plates with hardcore, the results predicted by the FSDT match well with the present solutions since the frequency ratio approaches unity. However, for FG sandwich plates with softcore, the FSDT overpredicts natural frequency (see Fig. 6), especially for higher values of power law index p.

4.2. Parameter studies

After verifying the accuracy of the present theory, parameter studies are carried out to investigate the influences of power law index p, thickness ratio of layers, i.e. scheme, and transverse shear deformation on deflection, critical buckling load and natural

frequency of FG sandwich plates. Numerical results are tabulated in Tables 10-12 and plotted in Figs. 7-16.

The effects of the power law index p on deflection, critical buckling load and fundamental natural frequency of FG sandwich square plates are illustrated in Figs. 7-9, respectively. The thickness ratio of the plate is taken equal to 10. It can be seen that increasing the power law index p results in an increase in deflection (see Fig. 7) and a reduction of buckling load (see Fig. 8) and natural frequency (see Fig. 9). This is due to the fact that higher power law index p corresponds to lower volume fraction of the ceramic phase V (see Fig. 2). In other word, increasing the power law index will reduce the stiffness of the plate due to high portion of metal in comparison with the ceramic part, and consequently, leads to an increase in deflection and a reduction of both buckling load and natural frequency. In addition, the effect of the power law index p on the through thickness variation of transverse shear stress $\bar{\sigma}_{xz}$ is also illustrated in Fig. 10 for (1-2-1) and (1-0-1) FG sandwich plates with $p=0$, 2, 5 and 8. It can be seen that, except for the case of homogeneous plates (i.e., $p=0$), the distributions of the transverse shear stress of (1-2-1) and (1-0-1) FG sandwich plates with $p=2$, 5 and 8 are almost the same. In other word, the variation of the power law index has negligible influence on the through thickness distribution of the transverse shear stress.

In order to investigate the effect of shear deformation on deflection, buckling load and natural frequency of FG sandwich plates, Figs. 11-13 display the variations of deflection, critical buckling load and fundamental frequency, respectively, with respect to thickness ratio a/h. The power law index is taken equal to 1. The dimensionless deflection, buckling load and frequency are obtained using the present theory and CPT. Since the CPT neglects the shear deformation, it underestimates deflection (see Fig. 11)

and overestimates buckling load (see Fig. 12) and natural frequency (see Fig. 13). The difference between the present theory and CPT is significant for thick to moderately thick FG sandwich plates, but it is negligible for thin plates with $a/h>20$. This means that the inclusion of shear deformation results in an increase in deflection and a reduction of both buckling load and natural frequency, and the effect of shear deformation is considerable for thick plates, but negligible for thin plates.

The effect of boundary conditions on deflection, buckling load and natural frequency is shown in Tables 10-12 and Figs. 14-16. It is observed that the hardest and softest plates correspond to the FCFC and SSSS ones, respectively. It is also noticeable from Table 10 and Fig. 7 that, for a constant power law index and thickness ratio, the lowest and highest values of deflection correspond to the (1-2-1) and (1-0-1) FG sandwich plates, respectively. Such behavior is due to the fact that the (1-2-1) and (1-0-1) FG sandwich plates correspond to the highest and lowest volume fractions of the ceramic phase V (see Fig. 2), and thus makes them become the hardest and softest ones.

5. Conclusions

A simple and accurate FSDT which eliminates the use of a shear correction factor was presented for FG sandwich plates composed of FG face sheets and an isotropic homogeneous core. Governing equations and boundary conditions are derived from Hamilton's principle. Analytical solutions for bending, buckling and free vibration analysis of simply supported plates are presented. Verification studies confirm that the present FSDT is not only more accurate than the conventional one, but also comparable with 3D elasticity theory and existing higher-order shear deformation theories which have a greater number of unknowns. In addition, the present FSDT is simpler than the conventional one due to having a fewer number of unknowns and governing equations,

and more importantly, it does not require a shear correction factor.

Acknowledgements

The second author gratefully acknowledges financial support from Vietnam National Foundation for Science and Technology Development (NAFOSTED) under Grant No. 107.02-2012.07.

References

[1] Zenkour AM. A comprehensive analysis of functionally graded sandwich plates: Part 1-Deflection and stresses. International Journal of Solids and Structures 2005;42(18–19):5224-5242.

[2] Zenkour AM. A comprehensive analysis of functionally graded sandwich plates: Part 2-Buckling and free vibration. International Journal of Solids and Structures 2005;42(18–19):5243-5258.

[3] Zenkour AM, Alghamdi NA. Thermoelastic bending analysis of functionally graded sandwich plates. Journal of Materials Science 2008;43(8):2574-2589.

[4] Zenkour AM, Alghamdi NA. Bending analysis of functionally graded sandwich plates under the effect of mechanical and thermal loads. Mechanics of Advanced Materials and Structures 2010;17(6):419-432.

[5] Zenkour AM, Sobhy M. Thermal buckling of various types of FGM sandwich plates. Composite Structures 2010;93(1):93-102.

[6] Reddy JN. A simple higher-order theory for laminated composite plates. Journal of Applied Mechanics 1984;51:745-752.

[7] Natarajan S, Manickam G. Bending and vibration of functionally graded material sandwich plates using an accurate theory. Finite Elements in Analysis and Design

2012;57:32-42.

[8] Neves AMA, Ferreira AJM, Carrera E, Cinefra M, Jorge RMN, Soares CMM. Static analysis of functionally graded sandwich plates according to a hyperbolic theory considering Zig-Zag and warping effects. Advances in Engineering Software 2012;52(0):30-43.

[9] Neves AMA, Ferreira AJM, Carrera E, Cinefra M, Jorge RMN, Soares CMM. Buckling analysis of sandwich plates with functionally graded skins using a new quasi-3D hyperbolic sine shear deformation theory and collocation with radial basis functions. ZAMM-Journal of Applied Mathematics and Mechanics 2012;92(9):749-766.

[10] Neves AMA, Ferreira AJM, Carrera E, Cinefra M, Roque CMC, Jorge RMN, et al. Static, free vibration and buckling analysis of isotropic and sandwich functionally graded plates using a quasi-3D higher-order shear deformation theory and a meshless technique. Composites Part B: Engineering 2013;44(1):657-674.

[11] Xiang S, Kang G-w, Yang M-s, Zhao Y. Natural frequencies of sandwich plate with functionally graded face and homogeneous core. Composite Structures 2013;96:226-231.

[12] Sobhy M. Buckling and free vibration of exponentially graded sandwich plates resting on elastic foundations under various boundary conditions. Composite Structures 2013;99:76-87.

[13] Thai HT, Choi DH. Zeroth-order shear deformation theory for functionally graded sandwich plates resting on elastic foundation. Composite Structures 2013;doi: 10.1016/j.compstruct.2013.09.055.

[14] Abdelaziz HH, Atmane HA, Mechab I, Boumia L, Tounsi A, Abbas ABE. Static

analysis of functionally graded sandwich plates using an efficient and simple refined theory. Chinese Journal of Aeronautics 2011;24(4):434-448.

[15] Ahmed Houari MS, Benyoucef S, Mechab I, Tounsi A, Adda Bedia EA. Two-variable refined plate theory for thermoelastic bending analysis of functionally graded sandwich plates. Journal of Thermal Stresses 2011;34(4):315-334.

[16] El Meiche N, Tounsi A, Ziane N, Mechab I, Adda.Bedia EA. A new hyperbolic shear deformation theory for buckling and vibration of functionally graded sandwich plate. International Journal of Mechanical Sciences 2011;53(4):237-247.

[17] Hadji L, Atmane HA, Tounsi A, Mechab I, Bedia EA. Free vibration of functionally graded sandwich plates using four-variable refined plate theory. Applied Mathematics and Mechanics 2011;32(7):925-942.

[18] Merdaci S, Tounsi A, Houari MSA, Mechab I, Hebali H, Benyoucef S. Two new refined shear displacement models for functionally graded sandwich plates. Archive of Applied Mechanics 2011;81(11):1507-1522.

[19] Bourada M, Tounsi A, Houari MSA. A new four-variable refined plate theory for thermal buckling analysis of functionally graded sandwich plates. Journal of Sandwich Structures and Materials 2012;14(1):5-33.

[20] Hamidi A, Zidi M, Houari MSA, Tounsi A. A new four variable refined plate theory for bending response of functionally graded sandwich plates under thermomechanical loading. Composites Part B: Engineering 2013;doi: 10.1016/j.compositesb.2012.03.021.

[21] Tounsi A, Houari MSA, Benyoucef S, Adda Bedia EA. A refined trigonometric shear deformation theory for thermoelastic bending of functionally graded sandwich plates. Aerospace Science and Technology 2013;24(1):209-220.

[22] Thai HT, Choi DH. A simple first-order shear deformation theory for the bending and free vibration analysis of functionally graded plates. Composite Structures 2013;101:332-340.

[23] Thai HT, Choi DH. A simple first-order shear deformation theory for laminated composite plates. Composite Structures 2013;106:754-763.

[24] Nguyen TK, Sab K, Bonnet G. First-order shear deformation plate models for functionally graded materials. Composite Structures 2008;83(1):25-36.

[25] Li Q, Iu VP, Kou KP. Three-dimensional vibration analysis of functionally graded material sandwich plates. Journal of Sound and Vibration 2008;311(1–2):498-515.

Figure Captions

Fig. 1. Geometry and coordinates of FG sandwich plates

Fig. 2. Variation of volume fraction of the ceramic phase V through the thickness

Fig. 3. Variation of dimensionless normal stress $\bar{\sigma}_x$ through the thickness of square plates ($a = 10h$)

Fig. 4. Variation of dimensionless transverse shear stress $\bar{\sigma}_{xz}$ through the thickness of square plates ($a = 10h$, $p = 2$)

Fig. 5. Comparison of dimensionless critical buckling load $\bar{N}$ of (1-2-1) FG sandwich rectangular plates ($b = 2a$, $p = 2$)

Fig. 6. Effect of shear correction factor on frequency of (1-2-1) FG sandwich square plates ($a = 5h$)

Fig. 7. Effect of power law index p on dimensionless deflection $\bar{w}$ of square plates ($a = 10h$)

Fig. 8. Effect of power law index p on dimensionless critical buckling load $\bar{N}$ of square plates under biaxial compression ($\gamma_1 = \gamma_2 = -1$, $a = 10h$)

Fig. 9. Effect of power law index p on dimensionless fundamental frequency $\bar{\omega}$ of square plates ($a = 10h$)

Fig. 10. Effect of the power law index p on the variation of transverse shear stress $\bar{\sigma}_{xz}$ through the thickness of square plates ($a = 10h$)

Fig. 11. Effect of shear deformation on dimensionless deflection $\bar{w}$ of square plates ($p = 1$)

Fig. 12. Effect of shear deformation on dimensionless critical buckling load $\bar{N}$ of square plates under biaxial compression ($\gamma_1 = \gamma_2 = -1$, $p = 1$)

Fig. 13. Effect of shear deformation on dimensionless fundamental frequency $\bar{\omega}$ of square plates ($p=1$)

Fig. 14. Effect of boundary conditions on dimensionless deflection $\bar{w}$ of (1-2-1) FG sandwich square plates ($p=1$)

Fig. 15. Effect of boundary conditions on dimensionless critical buckling load $\bar{N}$ of (1-2-1) FG sandwich square plates under biaxial compression ($p=1$)

Fig. 16. Effect of boundary conditions on dimensionless fundamental frequency $\bar{\omega}$ of (1-2-1) FG sandwich square plates ($p=1$)

Table Captions

Table 1. The admissible functions $X(x)$ and $Y(y)$

Table 2. Dimensionless deflection $\hat{w}$ of square plates ($a/h=10$)

Table 3. Dimensionless normal stress $\bar{\sigma}_x(h/2)$ of square plates ($a/h=10$)

Table 4. Dimensionless transverse shear stress $\bar{\sigma}_{xz}(0)$ of square plates ($a/h=10$)

Table 5. Dimensionless buckling load $\bar{N}$ of square plates under uniaxial compression ($\gamma_1=-1,\gamma_2=0$, $a/h=10$)

Table 6. Dimensionless buckling load $\bar{N}$ of square plates under biaxial compression ($\gamma_1=\gamma_2=-1$, $a/h=10$)

Table 7. Dimensionless fundamental frequency $\bar{\omega}$ of square plates ($a/h=10$)

Table 8. The first ten dimensionless frequencies $\bar{\omega}$ of square plates ($a/h=10$, $p=2$)

Table 9. Dimensionless fundamental frequency $\bar{\omega}$ of square thick plates ($a/h=5$)

Table 10. Dimensionless deflection $\bar{w}$ of square plates ($a/h=10$)

Table 11. Dimensionless buckling load $\bar{N}$ of square plates ($\gamma_1=\gamma_2=-1, a/h=10$)

Table 12. Dimensionless fundamental frequency $\bar{\omega}$ of square plates ($a/h=10$)

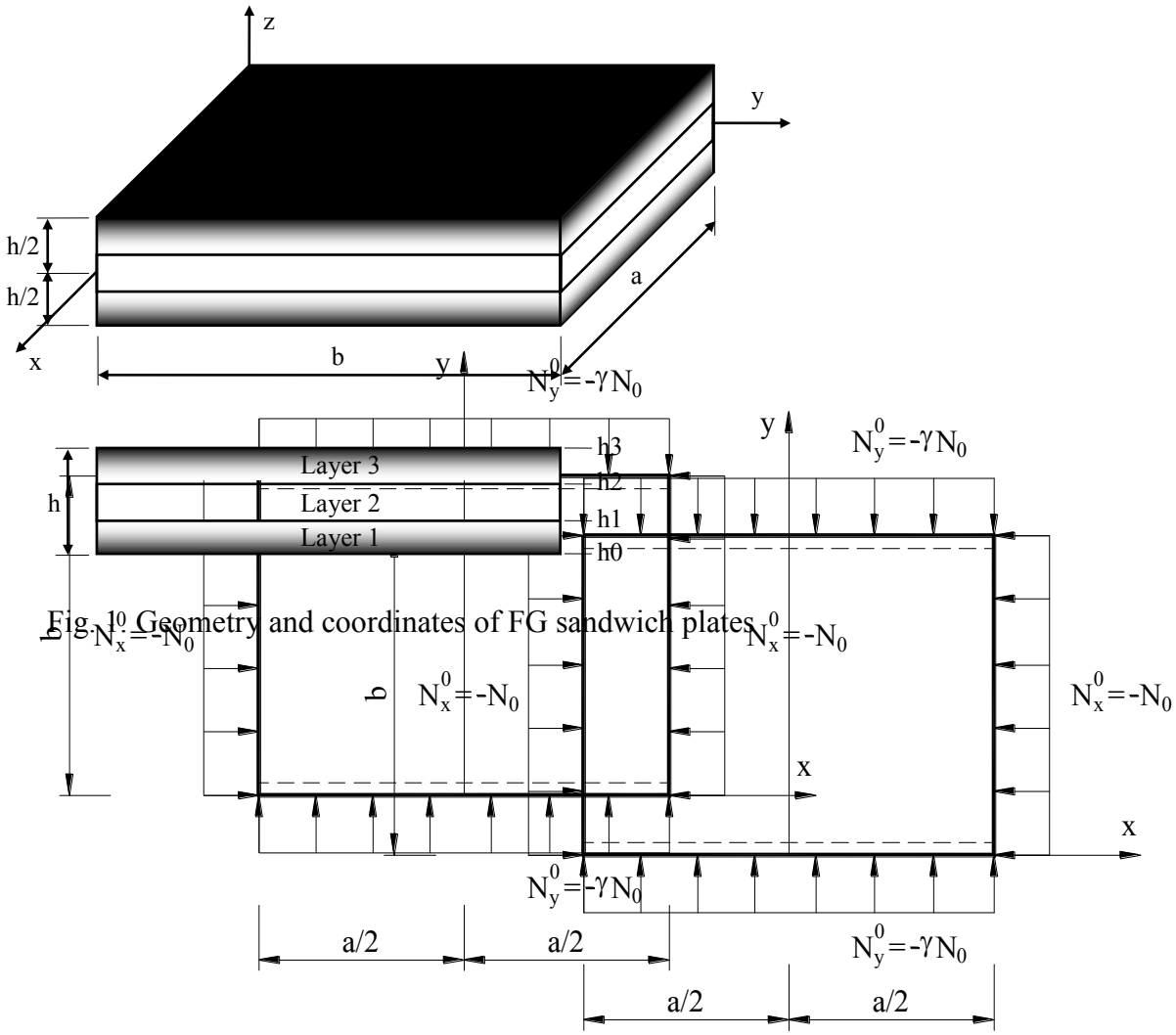

Fig. 1 Geometry and coordinates of FG sandwich plates

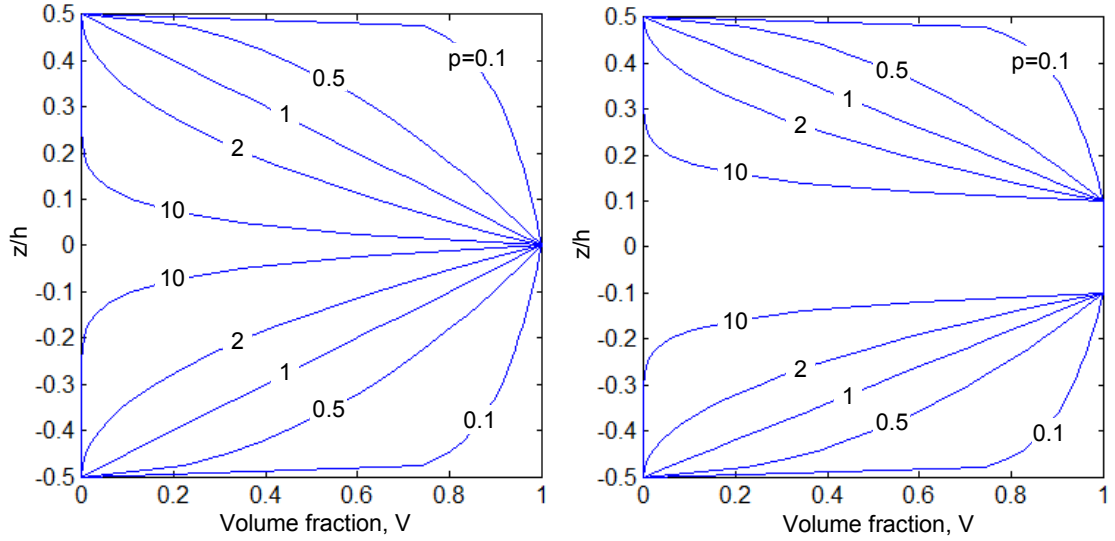

(a) 1-0-1

(b) 2-1-2

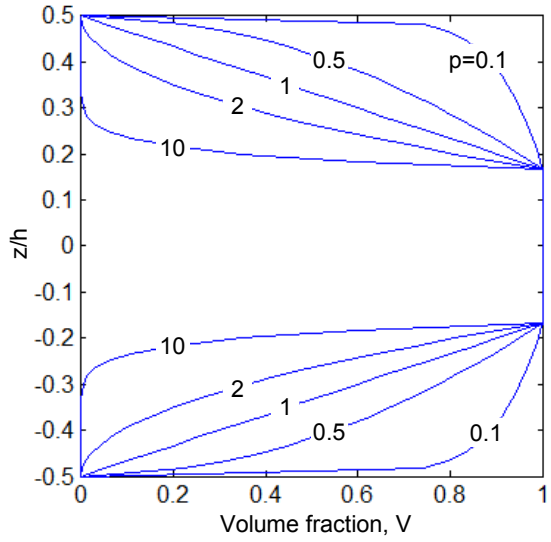

(c) 1-1-1

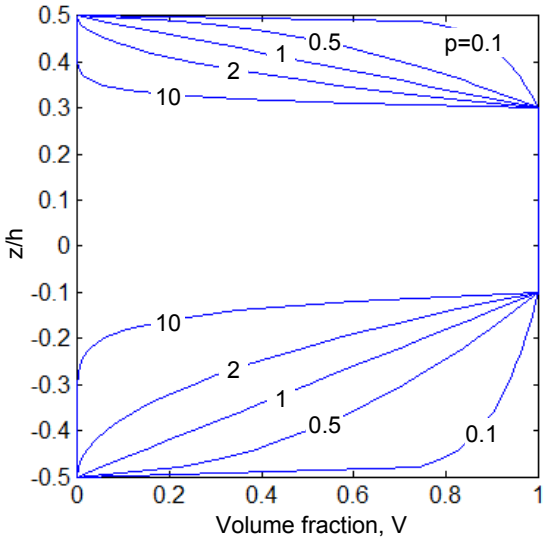

(d) 2-2-1

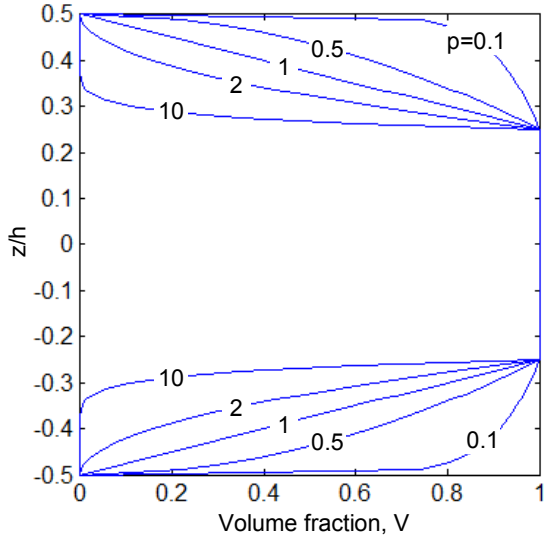

(e) 1-2-1

Fig. 2. Variation of volume fraction of the ceramic phase V through the thickness

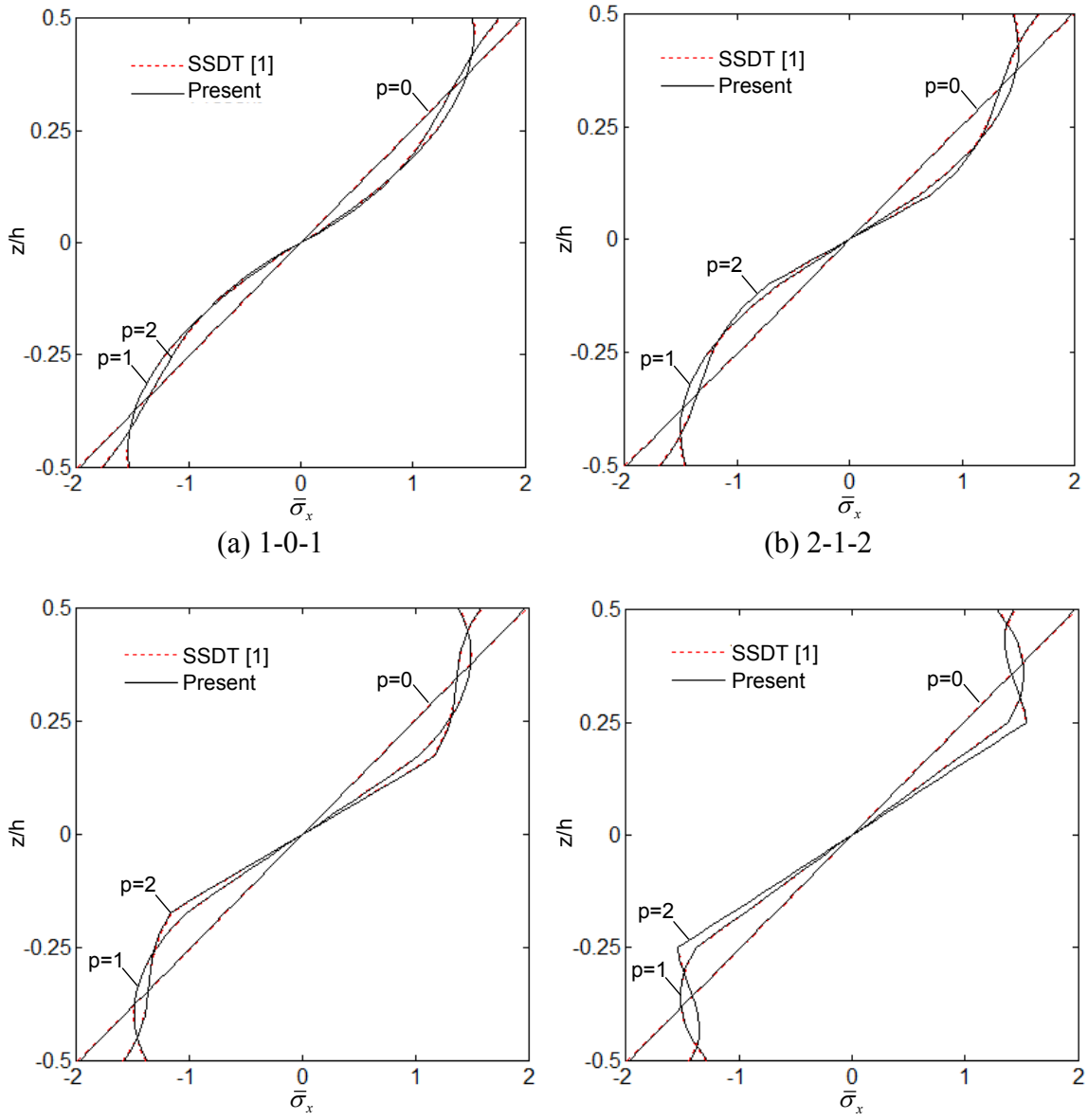

(a) 1-0-1 (b) 2-1-2

(c) 1-1-1 (d) 1-2-1

Fig. 3. Variation of dimensionless normal stress $\bar{\sigma}_x$ through the thickness of square plates ($a = 10h$)

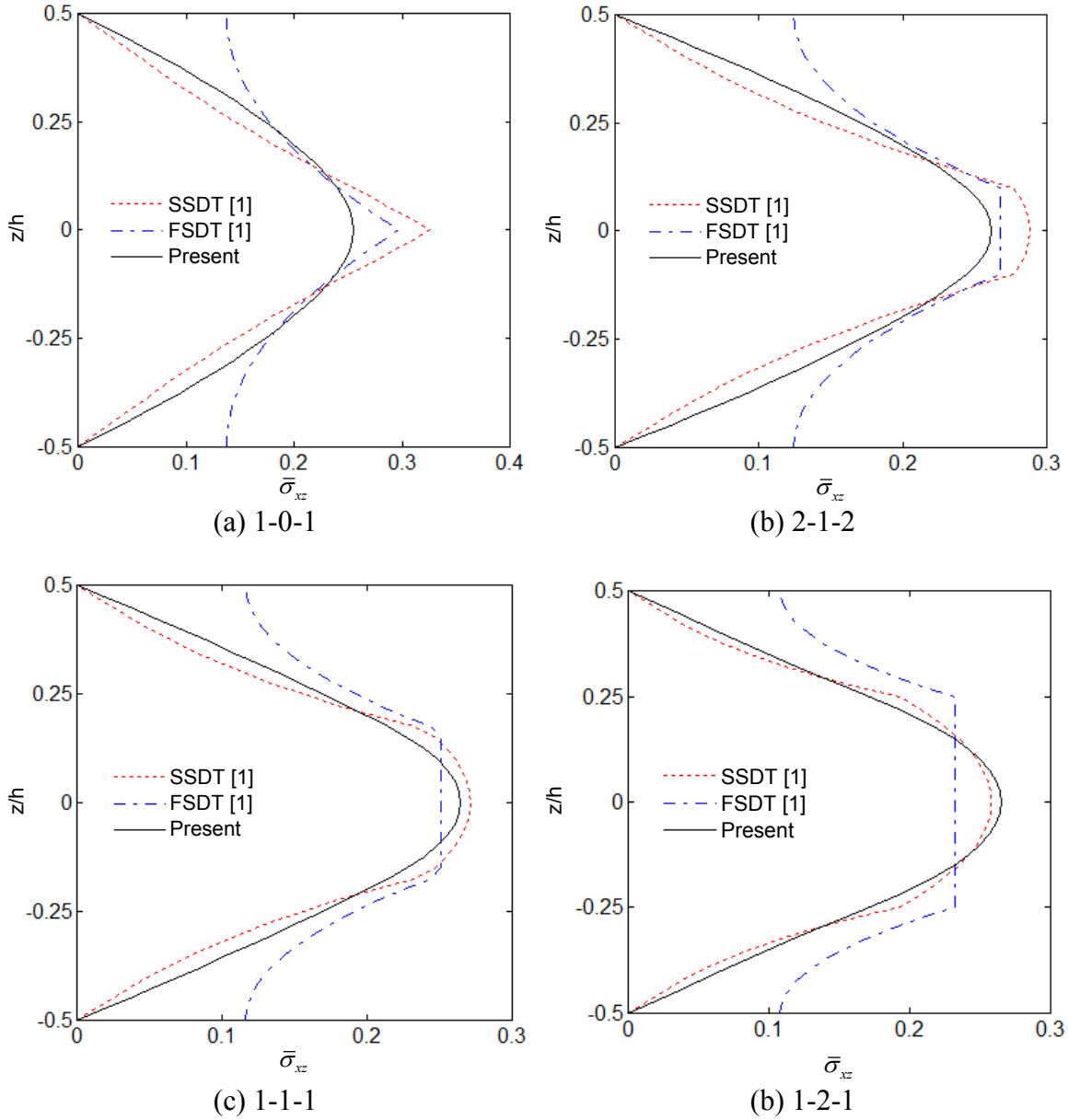

(a) 1-0-1 (b) 2-1-2

(c) 1-1-1 (b) 1-2-1

Fig. 4. Variation of dimensionless transverse shear stress $\bar{\sigma}_{xz}$ through the thickness of square plates ($a = 10h$, $p = 2$)

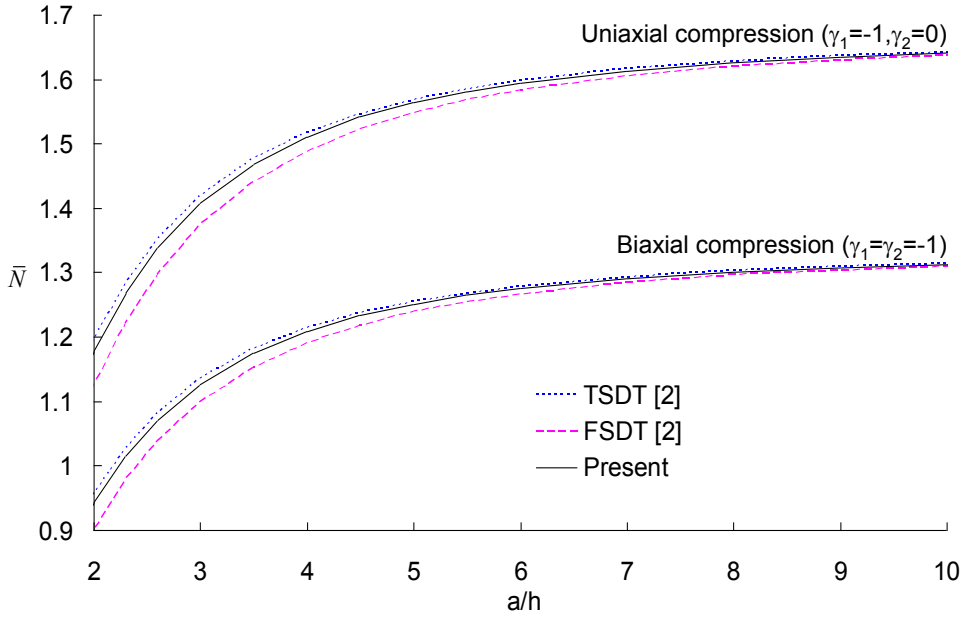

Fig. 5. Comparison of dimensionless critical buckling load $\bar{N}$ of (1-2-1) FG sandwich rectangular plates ($b = 2a$, $p = 2$)

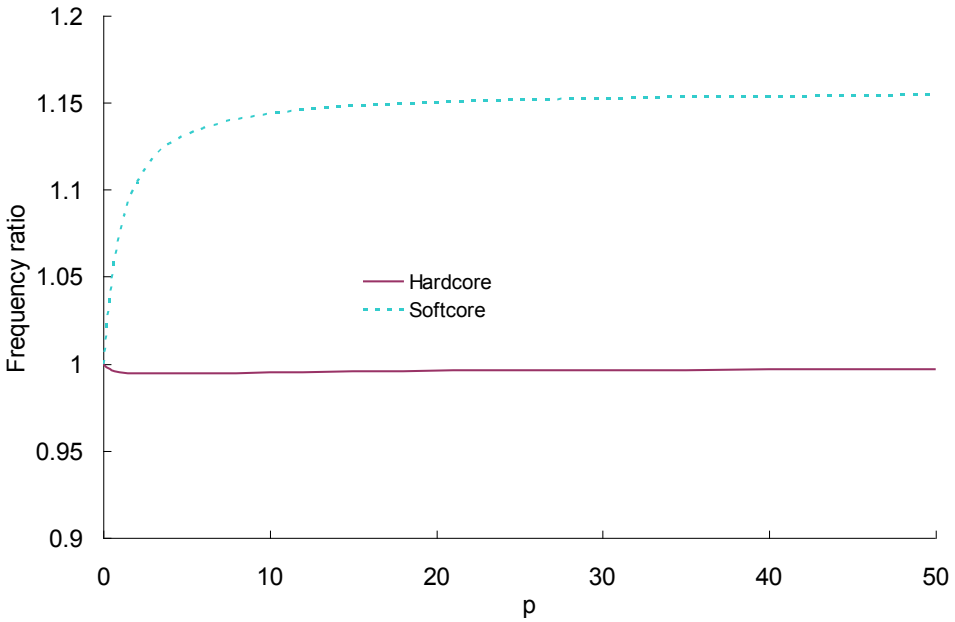

Fig. 6. Effect of shear correction factor on frequency of (1-2-1) FG sandwich square plates ($a = 5h$)

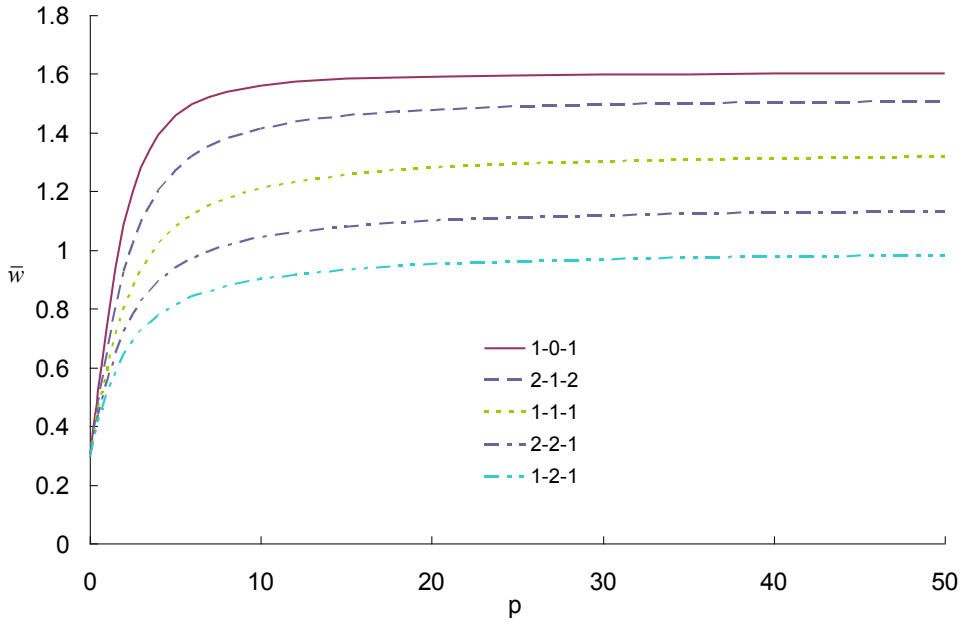

Fig. 7. Effect of power law index p on dimensionless deflection $\bar{w}$ of square plates ($a=10h$)

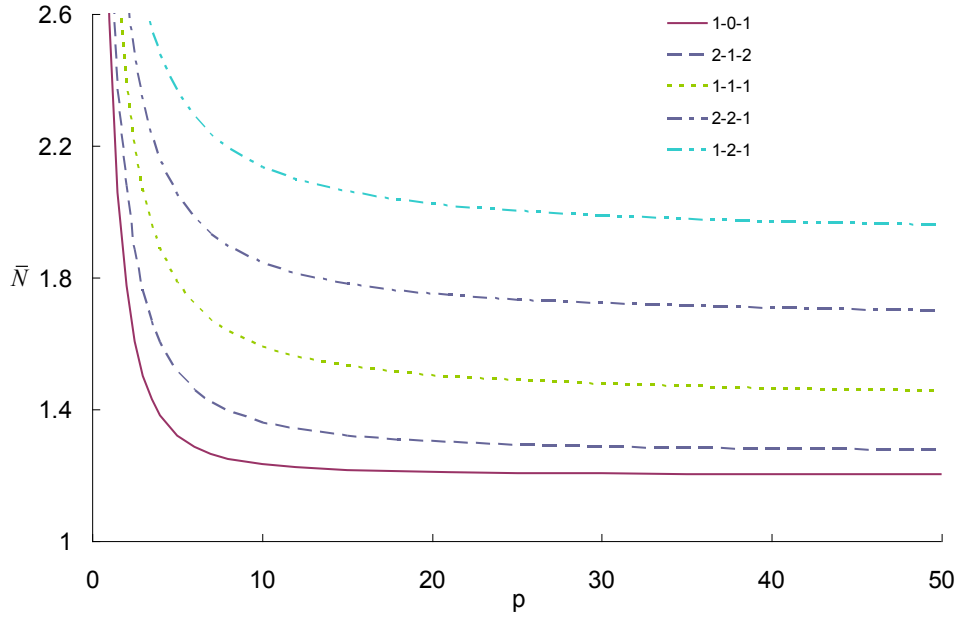

Fig. 8. Effect of power law index p on dimensionless critical buckling load $\bar{N}$ of square plates under biaxial compression ($\gamma_1=\gamma_2=-1, a=10h$)

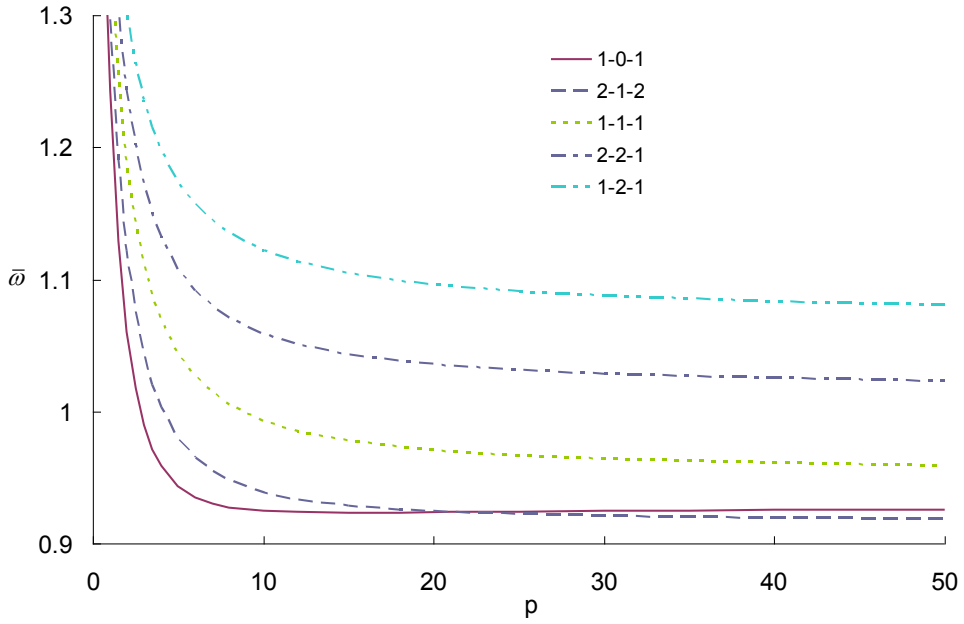

Fig. 9. Effect of power law index p on dimensionless fundamental frequency $\bar{\omega}$ of square plates ($a=10h$)

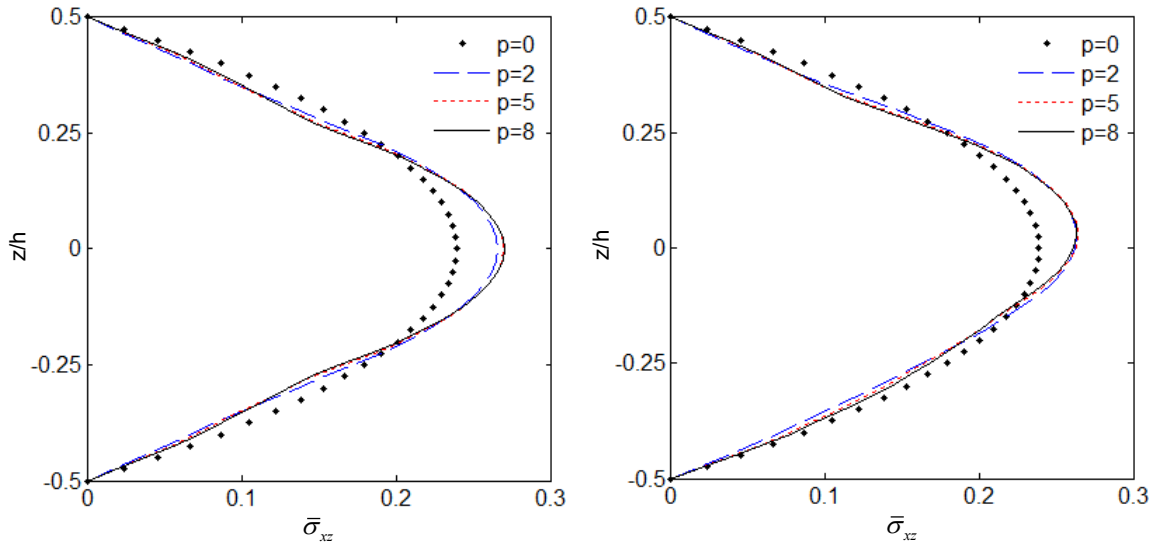

(a) 1-2-1 (b) 2-2-1

Fig. 10. Effect of the power law index p on the variation of transverse shear stress $\bar{\sigma}_{xz}$ through the thickness of square plates ($a=10h$)

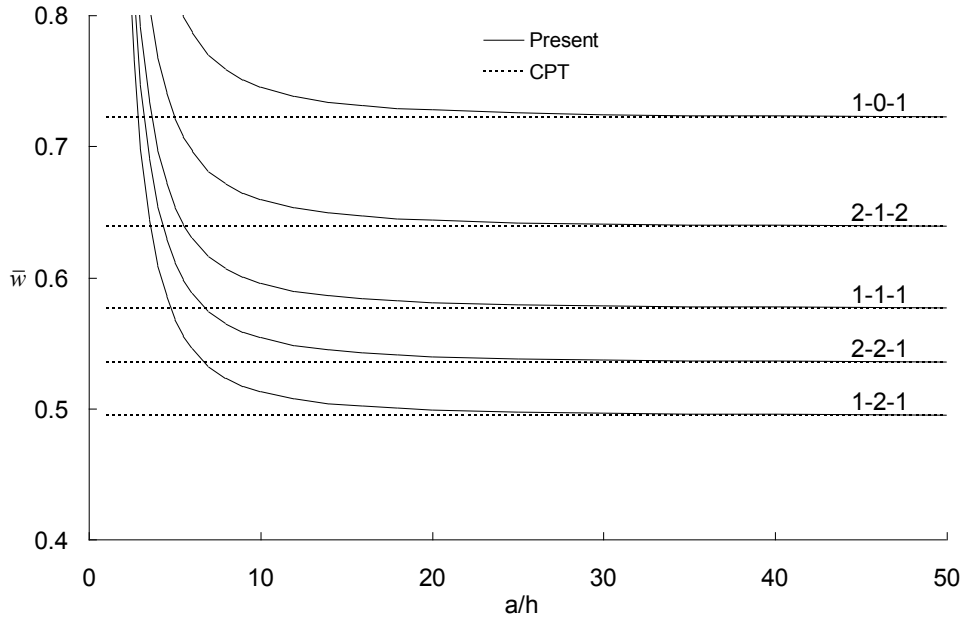

Fig. 11. Effect of shear deformation on dimensionless deflection $\bar{w}$ of square plates ($p=1$)

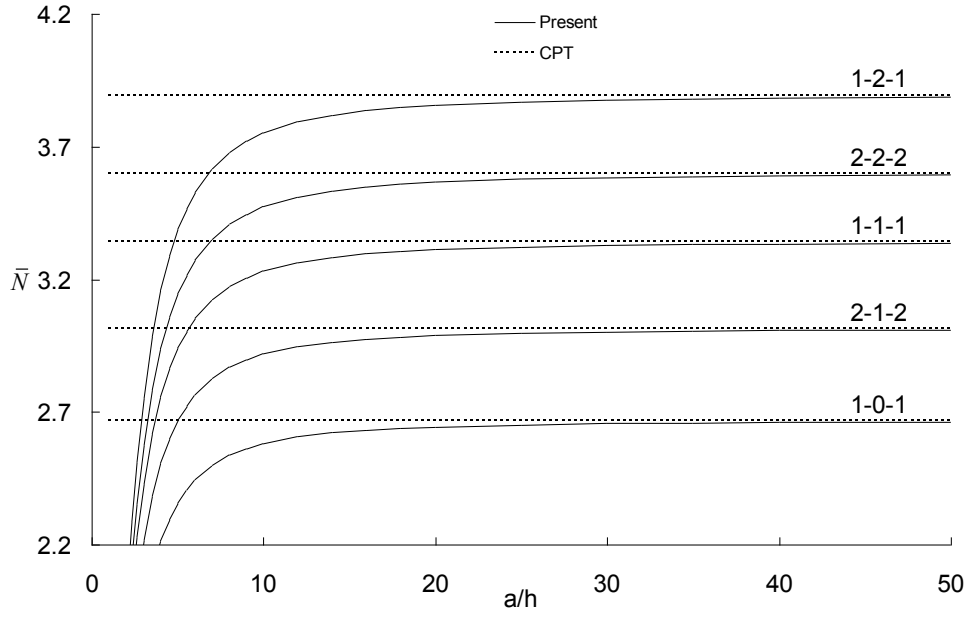

Fig. 12. Effect of shear deformation on dimensionless critical buckling load $\bar{N}$ of square plates under biaxial compression ($\gamma_1=\gamma_2=-1$, $p=1$)

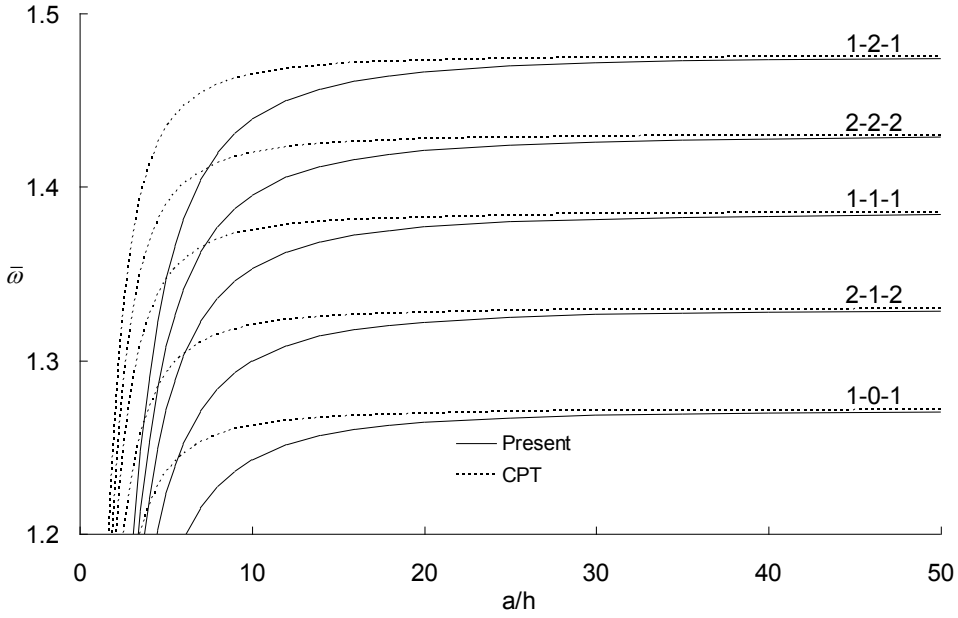

Fig. 13. Effect of shear deformation on dimensionless fundamental frequency $\bar{\omega}$ of square plates ($p=1$)

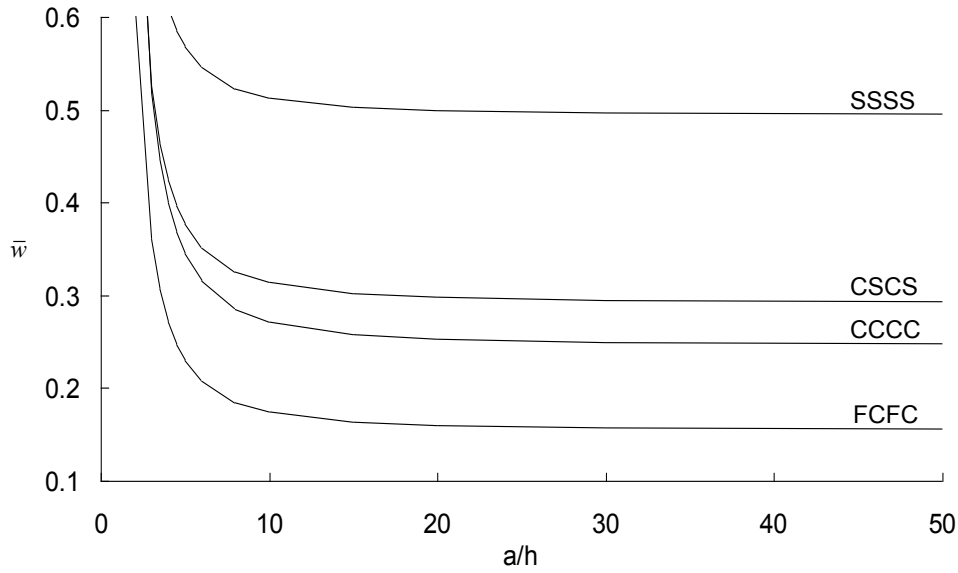

Fig. 14. Effect of boundary conditions on dimensionless deflection $\bar{w}$ of (1-2-1) FG sandwich square plates ($p=1$)

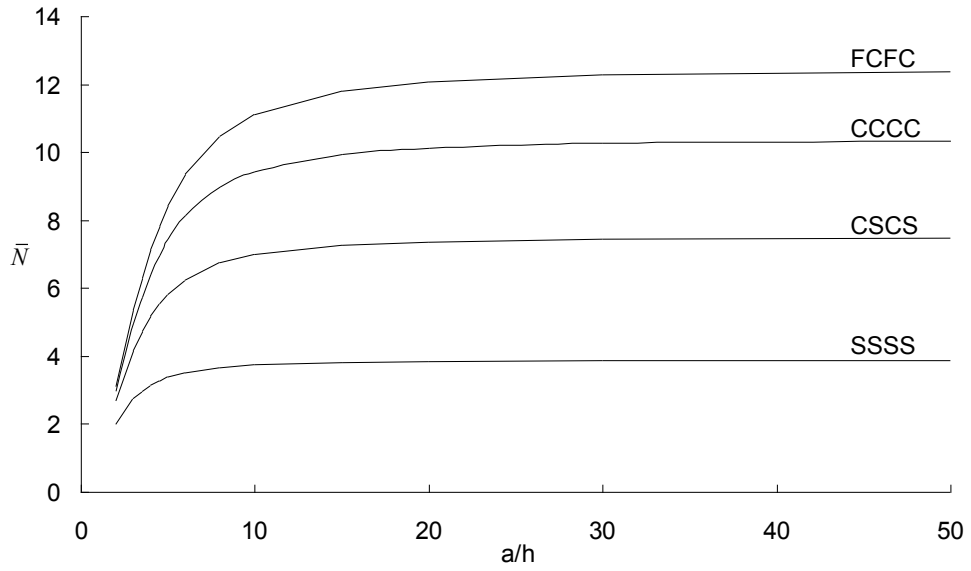

Fig. 15. Effect of boundary conditions on dimensionless critical buckling load $\bar{N}$ of (1-2-1) FG sandwich square plates under biaxial compression ($p=1$)

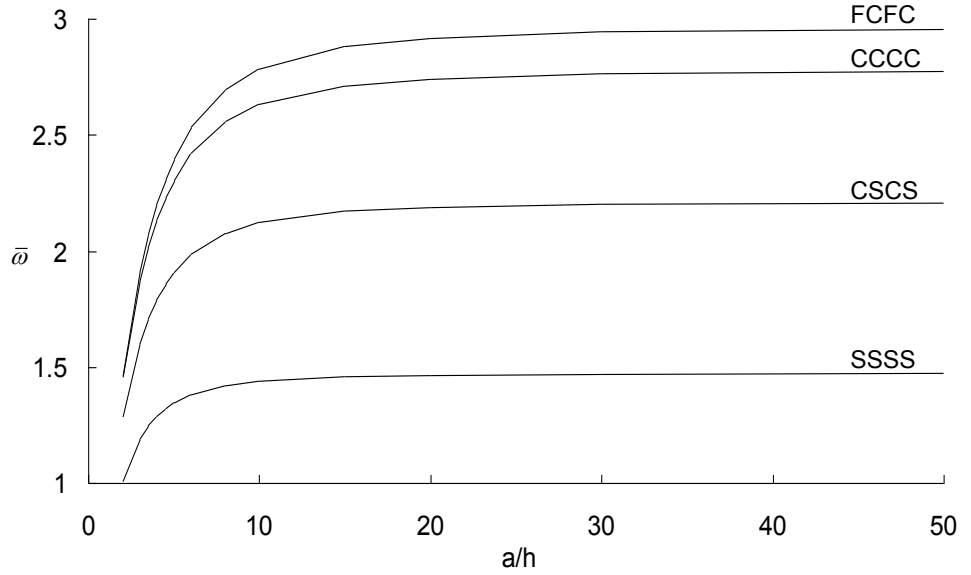

Fig. 16. Effect of boundary conditions on dimensionless fundamental frequency $\bar{\omega}$ of (1-2-1) FG sandwich square plates ($p=1$)

Table 1. The admissible functions $X(x)$ and $Y(y)$

Boundary conditions					The functions $X(x)$ and $Y(y)$	
Notation	$x=0$	$y=0$	$x=a$	$y=b$	$X(x)$	$Y(y)$
SSSS	S	S	S	S	$\sin(\alpha x)$	$\sin(\beta y)$
CSCS	C	S	C	S	$\sin^2(\alpha x)$	$\sin(\beta y)$
CCCC	C	C	C	C	$\sin^2(\alpha x)$	$\sin^2(\beta y)$
FCFC	F	C	F	C	$\cos^2(\alpha x)\left[\sin^2(\alpha x)+1\right]$	$\sin^2(\beta y)$

Table 2. Dimensionless deflection $\hat{w}$ of square plates ($a/h=10$)

p	Theory	Scheme				
		1-0-1	2-1-2	1-1-1	2-2-1	1-2-1
0	SSDT [1]	0.1961	0.1961	0.1961	0.1961	0.1961
	TSDT [1]	0.1961	0.1961	0.1961	0.1961	0.1961
	FSDT [1]	0.1961	0.1961	0.1961	0.1961	0.1961
	Present	0.1961	0.1961	0.1961	0.1961	0.1961
1	SSDT [1]	0.3235	0.3062	0.2919	0.2808	0.2709
	TSDT [1]	0.3236	0.3063	0.2920	0.2809	0.2709
	FSDT [1]	0.3248	0.3075	0.2930	0.2817	0.2717
	Present	0.3237	0.3064	0.2920	0.2809	0.2710
2	SSDT [1]	0.3732	0.3522	0.3328	0.3161	0.3026
	TSDT [1]	0.3734	0.3523	0.3329	0.3162	0.3026
	FSDT [1]	0.3751	0.3541	0.3344	0.3174	0.3037
	Present	0.3737	0.3526	0.3330	0.3163	0.3027
5	SSDT [1]	0.4091	0.3916	0.3713	0.3495	0.3347
	TSDT [1]	0.4093	0.3918	0.3715	0.3496	0.3348
	FSDT [1]	0.4112	0.3942	0.3736	0.3512	0.3363
	Present	0.4101	0.3927	0.3720	0.3501	0.3350
10	SSDT [1]	0.4175	0.4037	0.3849	0.3492	0.3412
	TSDT [1]	0.4177	0.4041	0.3855	0.3622	0.3482
	FSDT [1]	0.4192	0.4066	0.3879	0.3640	0.3500
	Present	0.3988	0.3894	0.3724	0.3492	0.3361

Table 3. Dimensionless normal stress $\bar{\sigma}_x\left(h/2\right)$ of square plates ($a/h=10$)

p	Theory	Scheme				
		1-0-1	2-1-2	1-1-1	2-2-1	1-2-1
0	SSDT [1]	2.0545	2.0545	2.0545	2.0545	2.0545
	TSDT [1]	2.0499	2.0499	2.0499	2.0499	2.0499
	FSDT [1]	1.9758	1.9758	1.9758	1.9758	1.9758
	Present	1.9758	1.9758	1.9758	1.9758	1.9758
1	SSDT [1]	1.5820	1.4986	1.4289	1.3234	1.3259
	TSDT [1]	1.5792	1.4959	1.4262	1.3206	1.3231
	FSDT [1]	1.5325	1.4517	1.3830	1.2775	1.2810
	Present	1.5324	1.4517	1.3830	1.2775	1.2810
2	SSDT [1]	1.8245	1.7241	1.6303	1.4739	1.4828
	TSDT [1]	1.8217	1.7214	1.6275	1.4710	1.4799
	FSDT [1]	1.7709	1.6750	1.5824	1.4253	1.4358
	Present	1.7709	1.6750	1.5824	1.4253	1.4358
5	SSDT [1]	1.9957	1.9155	1.8184	1.6148	1.6411
	TSDT [1]	1.9927	1.9130	1.8158	1.6118	1.6381
	FSDT [1]	1.9358	1.8648	1.7699	1.5640	1.5931
	Present	1.9358	1.8648	1.7699	1.5640	1.5931
10	SSDT [1]	2.0336	1.9731	1.8815	1.6198	1.6485
	TSDT [1]	2.0304	1.9713	1.8838	1.6666	1.7042
	FSDT [1]	1.9678	1.9217	1.8375	1.6165	1.6584
	Present	1.9678	1.9216	1.8375	1.6160	1.6587

Table 4. Dimensionless transverse shear stress $\bar{\sigma}_{xz}\left(0\right)$ of square plates ($a/h=10$)

p	Theory	Scheme				
		1-0-1	2-1-2	1-1-1	2-2-1	1-2-1
0	SSDT [1]	0.2462	0.2462	0.2462	0.2462	0.2462
	TSDT [1]	0.2386	0.2386	0.2386	0.2386	0.2386
	FSDT [1]	0.1910	0.1910	0.1910	0.1910	0.1910
	Present	0.2387	0.2387	0.2387	0.2387	0.2387
1	SSDT [1]	0.2991	0.2777	0.2681	0.2668	0.2600
	TSDT [1]	0.2920	0.2710	0.2612	0.2595	0.2526
	FSDT [1]	0.2610	0.2432	0.2326	0.2276	0.2206
	Present	0.2566	0.2593	0.2602	0.2582	0.2593
2	SSDT [1]	0.3329	0.2942	0.2781	0.2763	0.2654
	TSDT [1]	0.3262	0.2884	0.2719	0.2694	0.2583
	FSDT [1]	0.2973	0.2675	0.2508	0.2432	0.2326
	Present	0.2552	0.2617	0.2650	0.2624	0.2655
5	SSDT [1]	0.3937	0.3193	0.2915	0.2890	0.2715
	TSDT [1]	0.3863	0.3145	0.2864	0.2827	0.2651
	FSDT [1]	0.3454	0.2973	0.2721	0.2610	0.2460
	Present	0.2468	0.2576	0.2649	0.2627	0.2694
10	SSDT [1]	0.4415	0.3364	0.2953	0.2967	0.2768
	TSDT [1]	0.4321	0.3324	0.2957	0.2908	0.2690
	FSDT [1]	0.3728	0.3132	0.2830	0.2700	0.2526
	Present	0.2419	0.2534	0.2627	0.2611	0.2698

Table 5. Dimensionless buckling load $\bar{N}$ of square plates under uniaxial compression ($\gamma_1 = -1, \gamma_2 = 0$, $a/h = 10$)

p	Theory	Scheme				
		1-0-1	2-1-2	1-1-1	2-2-1	1-2-1
0	HSDT [16]	13.0055	13.0055	13.0055	13.0055	13.0055
	SSDT [2]	13.0061	13.0061	13.0061	13.0061	13.0061
	TSDT [2]	13.0050	13.0050	13.0050	13.0050	13.0050
	FSDT [2]	13.0045	13.0045	13.0045	13.0045	13.0045
	Present	13.0045	13.0045	13.0045	13.0045	13.0045
0.5	HSDT [16]	7.3638	7.9405	8.4365	8.8103	9.2176
	SSDT [2]	7.3657	7.9420	8.4371	8.8104	9.2167
	TSDT [2]	7.3644	7.9408	8.4365	8.8100	9.2168
	FSDT [2]	7.3373	7.9132	8.4103	8.7867	9.1952
	Present	7.3634	7.9403	8.4361	8.8095	9.2162
1	HSDT [16]	5.1663	5.8394	6.4645	6.9495	7.5072
	SSDT [2]	5.1685	5.8412	6.4654	6.9498	7.5063
	TSDT [2]	5.1671	5.8401	6.4647	6.9494	7.5066
	FSDT [2]	5.1424	5.8138	6.4389	6.9257	7.4837
	Present	5.1648	5.8387	6.4641	6.9485	7.5056
5	HSDT [16]	2.6568	3.0414	3.5787	4.1116	4.7346
	SSDT [2]	2.6601	3.0441	3.5806	4.1129	4.7349
	TSDT [2]	2.6582	3.0426	3.5796	4.1121	4.7347
	FSDT [2]	2.6384	3.0225	3.5596	4.0929	4.7148
	Present	2.6415	3.0282	3.5710	4.1024	4.7305
10	HSDT [16]	2.4857	2.7450	3.1937	3.7069	4.2796
	SSDT [2]	2.4893	2.7484	3.1946	3.1457	4.3818
	TSDT [2]	2.4873	2.7463	3.1947	3.7075	4.2799
	FSDT [2]	2.4690	2.7263	3.1752	3.6889	4.2604
	Present	2.4666	2.7223	3.1795	3.6901	4.2728

Table 6. Dimensionless buckling load $\bar{N}$ of square plates under biaxial compression ($\gamma_1 = \gamma_2 = -1,\ a/h = 10$)

p	Theory	Scheme				
		1-0-1	2-1-2	1-1-1	2-2-1	1-2-1
0	HSDT [16]	6.5028	6.5028	6.5028	6.5028	6.5028
	SSDT [2]	6.5030	6.5030	6.5030	6.5030	6.5030
	TSDT [2]	6.5025	6.5025	6.5025	6.5025	6.5025
	FSDT [2]	6.5022	6.5022	6.5022	6.5022	6.5022
	Present	6.5022	6.5022	6.5022	6.5022	6.5022
0.5	HSDT [16]	3.6819	3.9702	4.2182	4.4051	4.6088
	SSDT [2]	3.6828	3.9710	4.2186	4.4052	4.6084
	TSDT [2]	3.6822	3.9704	4.2182	4.4050	4.6084
	FSDT [2]	3.6687	3.9566	4.2052	4.3934	4.5976
	Present	3.6817	3.9702	4.2181	4.4047	4.6081
1	HSDT [16]	2.5832	2.9197	3.2323	3.4748	3.7536
	SSDT [2]	2.5842	2.9206	3.2327	3.4749	3.7531
	TSDT [2]	2.5836	2.9200	3.2324	3.4747	3.7533
	FSDT [2]	2.5712	2.9069	3.2195	3.4629	3.7418
	Present	2.5824	2.9193	3.2320	3.4742	3.7528
5	HSDT [16]	1.3284	1.5207	1.7894	2.0558	2.3673
	SSDT [2]	1.3300	1.5220	1.7903	2.0564	2.3674
	TSDT [2]	1.3291	1.5213	1.7898	2.0561	2.3673
	FSDT [2]	1.3192	1.5113	1.7798	2.0464	2.3574
	Present	1.3208	1.5141	1.7855	2.0512	2.3652
10	HSDT [16]	1.2429	1.3725	1.5969	1.8534	2.1398
	SSDT [2]	1.2448	1.3742	1.5973	1.5729	2.1909
	TSDT [2]	1.2436	1.3732	1.5974	1.8538	2.1400
	FSDT [2]	1.2345	1.3631	1.5876	1.8445	2.1302
	Present	1.2333	1.3612	1.5897	1.8450	2.1364

Table 7. Dimensionless fundamental frequency $\bar{\omega}$ of square plates ($a/h=10$)

p	Theory	Scheme				
		1-0-1	2-1-2	1-1-1	2-2-1	1-2-1
0	3D [25]	1.8268	1.8268	1.8268	1.8268	1.8268
	HSDT [16]	1.8245	1.8245	1.8245	1.8245	1.8245
	SSDT [2]	1.8245	1.8245	1.8245	1.8245	1.8245
	TSDT [2]	1.8245	1.8245	1.8245	1.8245	1.8245
	FSDT [2]	1.8244	1.8244	1.8244	1.8244	1.8244
	Present	1.8244	1.8244	1.8244	1.8244	1.8244
0.5	3D [25]	1.4461	1.4861	1.5213	1.5493	1.5767
	HSDT [16]	1.4442	1.4841	1.5192	1.5471	1.5746
	SSDT [2]	1.4444	1.4842	1.5193	1.5520	1.5745
	TSDT [2]	1.4442	1.4841	1.5192	1.5520	1.5727
	FSDT [2]	1.4417	1.4816	1.5170	1.5500	1.5727
	Present	1.4442	1.4841	1.5192	1.5471	1.5745
1	3D [25]	1.2447	1.3018	1.3552	1.3976	1.4414
	HSDT [16]	1.2431	1.3000	1.3533	1.3956	1.4394
	SSDT [2]	1.2434	1.3002	1.3534	1.4079	1.4393
	TSDT [2]	1.2432	1.3001	1.3533	1.4079	1.4393
	FSDT [2]	1.2403	1.2973	1.3507	1.4056	1.4372
	Present	1.2429	1.3000	1.3533	1.3956	1.4393
5	3D [25]	0.9448	0.9810	1.0453	1.1098	1.1757
	HSDT [16]	0.9457	0.9817	1.0446	1.1088	1.1740
	SSDT [2]	0.9463	0.9821	1.0448	1.1474	1.1740
	TSDT [2]	0.9460	0.9818	1.0447	1.1473	1.1740
	FSDT [2]	0.9426	0.9787	1.0418	1.1447	1.1716
	Present	0.9431	0.9796	1.0435	1.1077	1.1735
10	3D [25]	0.9273	0.9408	0.9952	1.0610	1.1247
	HSDT [16]	0.9281	0.9428	0.9954	1.0608	1.1231
	SSDT [2]	0.9288	0.9433	0.9952	1.0415	1.1346
	TSDT [2]	0.9284	0.9430	0.9955	1.1053	1.1231
	FSDT [2]	0.9251	0.9396	0.9926	1.1026	1.1207
	Present	0.9246	0.9390	0.9932	1.0587	1.1223

Table 8. The first ten dimensionless frequencies $\bar{\omega}$ of square plates ($a/h=10$, $p=2$)

Scheme	Mode (m,n)	Theory				
		HSDT [16]	SSDT [2]	TSDT [2]	FSDT [2]	Present
1-2-1	1 (1,1)	1.3025	1.3024	1.3025	1.3002	1.3023
	2 (1,2)	3.1573	3.1569	3.1570	3.1445	3.1563
	3 (2,2)	4.9098	4.9085	4.9088	4.8802	4.9079
	4 (1,3)	6.0289	6.0262	6.0267	5.9849	6.0262
	5 (2,3)	7.6415	7.6360	7.6367	7.5722	7.6384
	6 (1,4)	9.6847	9.6712	9.6723	9.5728	9.6811
	7 (3,3)	10.1782	10.1619	10.1631	10.0542	10.1746
	8 (2,4)	11.1464	11.1232	11.1246	10.9961	11.1430
	9 (3,4)	13.4665	13.4176	13.4194	13.2380	13.4640
	10 (4,4)	16.5069	16.3982	16.4004	16.1372	16.5076
2-2-1	1 (1,1)	1.2438	1.2678	1.2678	1.2652	1.2436
	2 (1,2)	3.0170	3.0738	3.0735	3.0597	3.0163
	3 (2,2)	4.6946	4.7807	4.7800	4.7482	4.6932
	4 (1,3)	5.7666	5.8702	5.8692	5.8226	5.7648
	5 (2,3)	7.3132	7.4400	7.4385	7.3664	7.3110
	6 (1,4)	9.2744	9.4255	9.4232	9.3120	9.2719
	7 (3,3)	9.7485	9.9044	9.9018	9.7801	9.7459
	8 (2,4)	10.6789	10.8426	10.8395	10.6959	10.6764
	9 (3,4)	12.9101	13.0826	13.0781	12.8754	12.9084
	10 (4,4)	15.8376	15.9939	15.9870	15.6935	15.8383

Table 9. Dimensionless fundamental frequency $\bar{\omega}$ of square thick plates ($a/h=5$)

p	Theory	Scheme				
		1-0-1	2-1-2	1-1-1	2-2-1	1-2-1
Hardcore						
0	3D [25]	1.6771	1.6771	1.6771	1.6771	1.6771
	Present	1.6697	1.6697	1.6697	1.6697	1.6697
	Present (k=5/6)	1.6697	1.6697	1.6697	1.6697	1.6697
0.5	3D [25]	1.3536	1.3905	1.4218	1.4454	1.4694
	Present	1.3473	1.3841	1.4152	1.4386	1.4626
	Present (k=5/6)	1.3395	1.3764	1.4081	1.4326	1.4571
1	3D [25]	1.1749	1.2292	1.2777	1.3143	1.3534
	Present	1.1691	1.2232	1.2714	1.3078	1.3467
	Present (k=5/6)	1.1607	1.2145	1.2632	1.3007	1.3403
5	3D [25]	0.8909	0.9336	0.9980	1.0561	1.1190
	Present	0.8853	0.9286	0.9916	1.0488	1.1118
	Present (k=5/6)	0.8836	0.9256	0.9862	1.0447	1.1056
10	3D [25]	0.8683	0.8923	0.9498	1.0095	1.0729
	Present	0.8599	0.8860	0.9428	1.0012	1.0648
	Present (k=5/6)	0.8613	0.8881	0.9406	1.0006	1.0596
Softcore						
0	3D [25]	0.8529	0.8529	0.8529	0.8529	0.8529
	Present	0.8491	0.8491	0.8491	0.8491	0.8491
	Present (k=5/6)	0.8491	0.8491	0.8491	0.8491	0.8491
0.5	3D [25]	1.3789	1.3206	1.2805	1.2453	1.2258
	Present	1.3686	1.3115	1.2729	1.2380	1.2185
	Present (k=5/6)	1.4242	1.3816	1.3423	1.2969	1.2766
1	3D [25]	1.5090	1.4333	1.3824	1.3420	1.3213
	Present	1.4915	1.4156	1.3702	1.3302	1.3104
	Present (k=5/6)	1.5626	1.5237	1.4835	1.4278	1.4101
5	3D [25]	1.6587	1.5801	1.5028	1.4601	1.4267
	Present	1.6305	1.5125	1.4589	1.4195	1.4026
	Present (k=5/6)	1.6774	1.6718	1.6491	1.5895	1.5876
10	3D [25]	1.6728	1.6091	1.5267	1.4831	1.4410
	Present	1.6495	1.5196	1.4642	1.4266	1.4101
	Present (k=5/6)	1.6778	1.6827	1.6672	1.6100	1.6130

Table 10. Dimensionless deflection $\bar{w}$ of square plates ($a/h=10$)

Boundary conditions	p	Scheme				
		1-0-1	2-1-2	1-1-1	2-2-1	1-2-1
SSSS	0	0.2961	0.2961	0.2961	0.2961	0.2961
	0.5	0.5229	0.4849	0.4564	0.4371	0.4178
	1	0.7455	0.6594	0.5956	0.5541	0.5130
	2	1.0846	0.9256	0.8011	0.7205	0.6433
	5	1.4576	1.2714	1.0782	0.9385	0.8139
	10	1.5609	1.4143	1.2109	1.0434	0.9011
CSCS	0	0.1841	0.1841	0.1841	0.1841	0.1841
	0.5	0.3208	0.2975	0.2803	0.2688	0.2571
	1	0.4547	0.4021	0.3636	0.3389	0.3141
	2	0.6593	0.5617	0.4865	0.4385	0.3920
	5	0.8900	0.7712	0.6529	0.5697	0.4940
	10	0.9595	0.8606	0.7339	0.6338	0.5464
CCCC	0	0.1612	0.1612	0.1612	0.1612	0.1612
	0.5	0.2780	0.2579	0.2431	0.2333	0.2233
	1	0.3923	0.3469	0.3140	0.2930	0.2718
	2	0.5674	0.4828	0.4184	0.3777	0.3380
	5	0.7685	0.6626	0.5603	0.4897	0.4247
	10	0.8327	0.7412	0.6302	0.5452	0.4693
FCFC	0	0.1043	0.1043	0.1043	0.1043	0.1043
	0.5	0.1786	0.1657	0.1563	0.1501	0.1437
	1	0.2513	0.2222	0.2012	0.1879	0.1744
	2	0.3628	0.3084	0.2674	0.2416	0.2164
	5	0.4925	0.4232	0.3575	0.3129	0.2713
	10	0.5355	0.4742	0.4023	0.3484	0.2997

Table 11. Dimensionless buckling load $\bar{N}$ of square plates ($\gamma_1 = \gamma_2 = -1$, $a / h = 10$)

Boundary conditions	p	Scheme				
		1-0-1	2-1-2	1-1-1	2-2-1	1-2-1
SSSS	0	6.5022	6.5022	6.5022	6.5022	6.5022
	0.5	3.6817	3.9702	4.2181	4.4047	4.6081
	1	2.5824	2.9193	3.2320	3.4742	3.7528
	2	1.7749	2.0798	2.4032	2.6719	2.9926
	5	1.3208	1.5141	1.7855	2.0512	2.3652
	10	1.2333	1.3612	1.5897	1.8450	2.1364
CSCS	0	11.9477	11.9477	11.9477	11.9477	11.9477
	0.5	6.8587	7.3942	7.8489	8.1861	8.5573
	1	4.8390	5.4712	6.0504	6.4925	7.0048
	2	3.3370	3.9170	4.5225	5.0176	5.6129
	5	2.4721	2.8529	3.3697	3.8622	4.4536
	10	2.2930	2.5565	2.9978	3.4713	4.0269
CCCC	0	15.9226	15.9226	15.9226	15.9226	15.9226
	0.5	9.2338	9.9529	10.5578	11.0011	11.4933
	1	6.5434	7.3990	8.1753	8.7612	9.4443
	2	4.5236	5.3169	6.1354	6.7961	7.5952
	5	3.3400	3.8738	4.5813	5.2417	6.0445
	10	3.0825	3.4629	4.0732	4.7084	5.4696
FCFC	0	18.6047	18.6047	18.6047	18.6047	18.6047
	0.5	10.8640	11.7085	12.4145	12.9276	13.5006
	1	7.7220	8.7323	9.6429	10.3246	11.1229
	2	5.3477	6.2913	7.2569	8.0294	8.9676
	5	3.9393	4.5849	5.4268	6.2015	7.1514
	10	3.6230	4.0915	4.8230	5.5683	6.4748

Table 12. Dimensionless fundamental frequency $\bar{\omega}$ of square plates ($a/h=10$)

Boundary conditions	p	Scheme				
		1-0-1	2-1-2	1-1-1	2-2-1	1-2-1
SSSS	0	1.8244	1.8244	1.8244	1.8244	1.8244
	0.5	1.4442	1.4841	1.5192	1.5471	1.5745
	1	1.2429	1.3000	1.3533	1.3956	1.4393
	2	1.0605	1.1218	1.1882	1.2436	1.3023
	5	0.9431	0.9796	1.0435	1.1077	1.1735
	10	0.9246	0.9390	0.9932	1.0587	1.1223
CSCS	0	2.6701	2.6701	2.6701	2.6701	2.6701
	0.5	2.1277	2.1862	2.2371	2.2768	2.3162
	1	1.8365	1.9209	1.9986	2.0593	2.1226
	2	1.5694	1.6616	1.7592	1.8394	1.9251
	5	1.3927	1.4512	1.5471	1.6405	1.7380
	10	1.3610	1.3889	1.4720	1.5672	1.6629
CCCC	0	3.2936	3.2936	3.2936	3.2936	3.2936
	0.5	2.6376	2.7099	2.7719	2.8199	2.8679
	1	2.2814	2.3864	2.4818	2.5556	2.6330
	2	1.9520	2.0680	2.1889	2.2868	2.3923
	5	1.7293	1.8064	1.9269	2.0415	2.1629
	10	1.6858	1.7268	1.8329	1.9497	2.0703
FCFC	0	3.4688	3.4688	3.4688	3.4688	3.4688
	0.5	2.7872	2.8634	2.9284	2.9781	3.0282
	1	2.4144	2.5256	2.6258	2.7027	2.7838
	2	2.0675	2.1914	2.3190	2.4215	2.5323
	5	1.8296	1.9145	2.0430	2.1632	2.2918
	10	1.7806	1.8285	1.9429	2.0656	2.1942